Biosensors and Bioelectronics: X 1 (2019) 100015

Contents lists available at ScienceDirect

Biosensors and Bioelectronics: X

journal homepage: www.journals.elsevier.com/biosensors-and-bioelectronics-x

Trends in the design of wavelength-based optical fibre biosensors (2008–2018)

A.B. Socorro-Leránoz[a,b,*], D. Santano[a], I. Del Villar[a,b], I.R. Matias[a,b]

[a] Department of Electrical, Electronic and Communication Engineering, Universidad Publica de Navarra (UPNA), Ed. Los Tejos, Campus of Arrosadia S/n, 31006, Pamplona, Spain

[b] Institute of Smart Cities, Jeronimo de Ayanz R&D Center, Campus of Arrosadia, 31006, Pamplona, Spain

ARTICLE INFO

Keywords:
Biosensors
Optical fibre
Interferometry
Fabry–Pérot
Fibre Bragg gratings
Long-period fibre Bragg gratings
Surface plasmon resonance
Localized surface plasmon resonance
Lossy mode resonance

ABSTRACT

During the last decades, both governments and companies have been committed to the continuous checking of biological parameters, which can prevent extra costs to administrations. A very efficient way to address this issue is by designing biosensors. This contribution reviews the advances made using optical fibre technology, which have lately agglutinated much of the scientific interest related to the development of biosensors. However, the wide number of publications describing the use of optical fibre for detecting biomarkers has probably blurred the main goal: obtaining portable, simple, easy-to-handle and cost-effective biosensors. With this purpose, this contribution presents some optical fibre structures which have been analysed in terms of several optical parameters of interest from a photonics point of view: sensitivity, quality factor, full width at half minimum, limit of detection and figure of merit. This has made it possible to classify the most advanced optical fibre sensing techniques and, hence, their suitability when developing biosensing applications.

1. Introduction

In recent decades, the biosensors market has experienced a great development, above all regarding medical healthcare (P&S Market Research, 2015). The principal causes motivating this situation are the increase of diabetes and the aging of the population, which can be corroborated currently in both developed and developing countries. Behind this market, major global companies, in collaboration with the different administrations, are clearly investing in producing applications that allow patients to manage their own health at home. At the same time, both companies and governments are promoting point-of-care testing and self-care applications rather than having patients saturating hospital waiting rooms. In this respect, the development of a recent type of sensor, known as biosensors, facilitates this work, since they are designed to detect a specific malfunction on time and therefore to help physicians heal patients. In fact, by summing the benefits obtained by the biosensors market when used in clinical diagnostics and medical instrumentation alone, 64% of the total market is covered, as indicated in Fig. 1.

However, healthcare is not the only application field of biosensors. The same report also highlights biosensing applications in the control of industrial processes (11%), veterinary and agriculture testing (8%), defence (6%), environmental applications (5%), research laboratories (3%) and robotics (2%), among others. According to the Scopus research browser, more than 66800 contributions related to biosensors have been written since the 1960s. In spite of this, for the sake of simplicity, this contribution will only focus on the development of biosensors for medical applications.

A biosensor detects a chemical or biochemical substance by transducing a biological interaction into a variation of any sort of signal that can be measured easily. Its structure consists of three clearly defined parts: the substrate, the biofunctionalization interface and the bioreceptors (Holzinger et al., 2014). Typical bioreceptors are, generally, antibodies, enzymes, proteins, aptamers, cells or microorganisms. All of them are specifically designed to detect other target molecules, also called “analytes” or “biomarkers”. The substrate transduces these biological interactions into measurable variables and converts them into optical, electrical, mechanical or acoustic signals that can be processed afterwards. Finally, the biofunctionalization interface is the intermediate layer. It consists of one or several sublayers that attach the bioreceptors to the substrate by means of nanotechnology-based techniques.

As is well known, there are numerous techniques to develop biosensors, such as those based on micro-(opto)-electromechanical systems

* Corresponding author. Department of Electrical, Electronic and Communication Engineering, Universidad Publica de Navarra (UPNA), Ed. Los Tejos, Campus of Arrosadia S/n, 31006 Pamplona, Spain.

E-mail address: ab.socorro@unavarra.es (A.B. Socorro-Leránoz).

https://doi.org/10.1016/j.biosx.2019.100015
Received 8 February 2019; Received in revised form 23 April 2019; Accepted 13 May 2019
Available online 31 May 2019

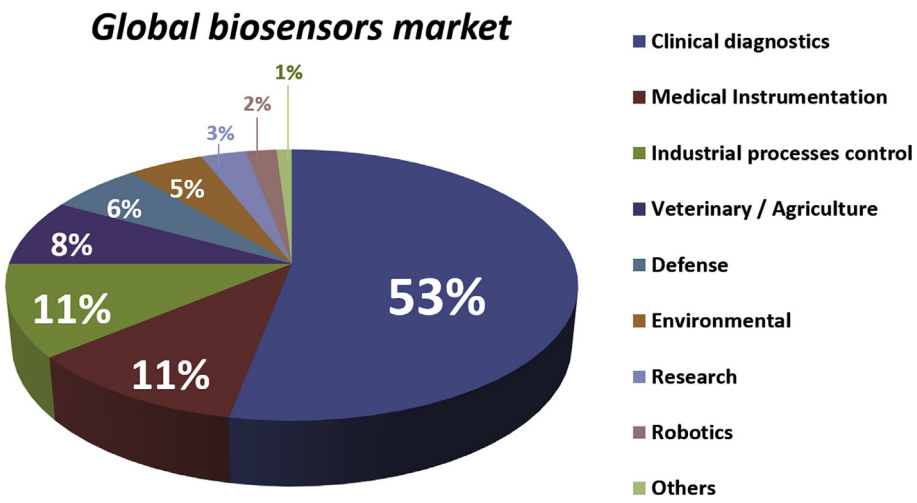

Fig. 1. Global biosensors market pie chart. 64% of the money involved in this market is due to activities related to medicine: home healthcare and point-of-care testing.

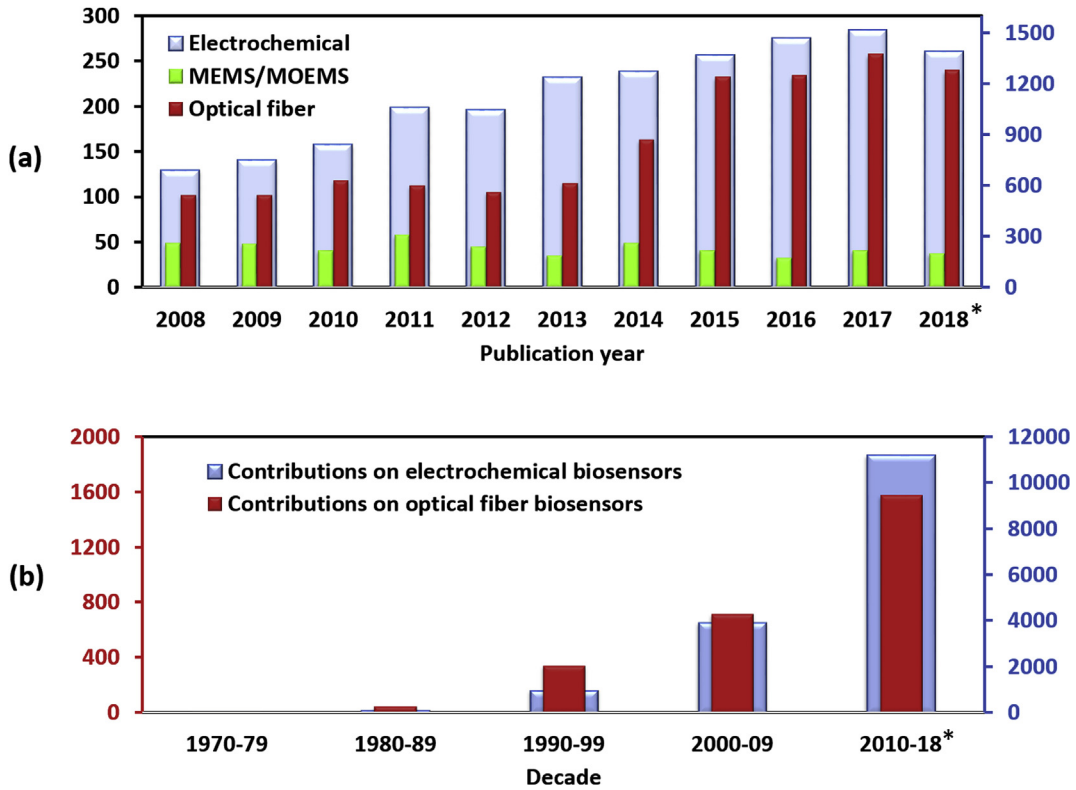

Fig. 2. Contributions related to different kinds of biosensing technologies (a search in Scopus by: "Electrochemical AND biosensor", "MEMS OR MOEMS AND biosensor" or "Optical fibre AND biosensor" was performed to obtain the data): (a) MEMS/MOEMS, electrochemical and optical fibres evolution from 2008 to 2018. (b) Comparison between the contributions related to electrochemical and optical fibre-based biosensors since the 1970s. *At the publication date, Scopus was probably still collecting and classifying the corresponding data for 2018, so the data presented here may not coincide with the exact values for this year.

(MEMS/MOEMS) (Alvarez and Lechuga, 2010), electrochemistry (Weltin et al., 2016) or optics (Hawk and Armani, 2015). The operating principle of MEMS is the detection of the mechanical vibrations experienced by tiny structures called microcantilevers as a function of the interaction between the bioreceptors and the target biomolecules. However, though they constitute a sensing technology with high potential, their current production cost is high and that is why they are still under research. In fact, Fig. 2a shows that the number of contributions related to MEMS/MOEMS has not increased during the last decade.

This is not the case of electrochemical biosensors, which are based on capturing the electrons released by redox reactions taking place between the analytes and the bioreceptors. Some of them are based on direct interactions between analytes and bioreceptors (Carneiro et al., 2017), whereas others are based on detecting the electrons released by an additional substance that takes advantage of the analyte-bioreceptor interaction to produce them (Yang et al., 2018). It is quite easy to functionalize electrodes specifically designed to address biodetection, since the manufacture of planar integrated electrical technology has experienced a wide expansion during the last decades. This has made this technology the most attractive in terms of costs and the most efficient in terms of reducing the limit of detection of the analytes.

Therefore, current electrochemical-based biosensors represent the only technology that is ready to satisfy the demands of the biosensors market. Concerning research, they have presented a sustained growth over the last 10 years, which indicates that this technology is being progressively improved (see Fig. 2a).

Regarding optical biosensors, they are the second most explored group. Some of the most relevant configurations are those based on photonic crystals (Gharsallah et al., 2018; Shafiee et al., 2014), optical resonators (rings, toroids, cylinders, spheres, …) (Pongruengkiat and Pechprasarn, 2017; Tavousi et al., 2018), integrated optics (planar waveguides, Mach–Zehnder or Michelson interferometers, …) (Nabok et al., 2019) and optical fibres. Focusing on optical fibres, the number of contributions over the last decades related to optical fibre biosensors has increased greatly, especially since 2013 (see Fig. 2a and b). This increasing interest can be partially explained by the progressive introduction of this technology in medicine. Nowadays, it is quite common to find optical fibres in interesting applications such as endoscopy (Krans, 2015), laser applications allowing the removal of varicose veins (Sroka et al., 2010) or to protect elderly men from benign prostatic hyperplasia (BPH) (Martyn-Hemphill et al., 2017). This success is explained by several properties that make optical fibres suitable for medical applications:

A. Biocompatibility: optical fibres are mostly made of silica and plastic. These materials seem not to present side-effects when interacting with or being immersed in biological substances (Monton et al., 2012; Jiang et al., 2018).
B. Reduced size, flexibility and low weight: these properties allow fibres to be introduced into the organism in order to illuminate its inner cavities (Rosenthal et al., 2014) or to monitor physical variables with a catheter (Carotenuto et al., 2018). In this way, it is feasible to reach places in the human body that are otherwise inaccessible without open surgery.
C. Low cost: the success of optical fibre-based communications has enabled the reduction of the manufacturing costs. Consequently, it is nowadays cheaper to develop medical equipment based on this technology.
D. Capability to work in hazardous media: optical fibre has demonstrated good performance working in nuclear environments (Cheymol et al., 2011) or in the ocean (Hou et al., 2015). Therefore, it is necessary to keep on optimizing the operation of this technology in complex biological matrices such as blood (Wang and Wolfbeis, 2016).
E. Electromagnetic interference (EMI) immunity: optical fibre sensors, unlike electrochemical sensors, are not affected by EMIs. The frequency variations of the electromagnetic fields surrounding the fibres are several orders of magnitude below the light frequencies propagated inside.
F. Multiparameter sensing: optical fibre has the ability to multiplex and integrate signals from different sensors in optical networks, in either time or wavelength domains (Lismont et al., 2014; Liu et al., 2016).
G. Diversity of light propagation configurations: the optical fibre, as a cable, guides the light, but it is possible to mould the light flux by modifying the fibre structure with different configurations (Zamarreño et al., 2015).

In connection with the latter property, researchers have defined the concept of "*lab on fibre*" (Principe et al., 2017; Vaiano et al., 2016), which comprises any kind of modifications, depositions, printing processes, etc., that can be done in, on and around the optical fibres to achieve biodetection. Basically, there are two main detection methods. The first one is based on monitoring light intensity changes at a determined wavelength. Here, absorption (Arnold, 1985) and luminescence (Elosua et al., 2015) are the most used techniques. They are quite simple to manage and, therefore, the most cost-effective. However, they have a major drawback, which is the need for a stable signal reference, since the sources may vary their intensity as a function of time. Some techniques have been developed for compensating this issue (Wang et al., 2001).

The second method is wavelength detection-based techniques. It is based on tracking the wavelength shift of the transmission or attenuation bands in the spectrum. These configurations are usually more robust with respect to intensity-based techniques, since they avoid the instability of optical intensity signals. However, they are more expensive, since they need a spectrometer or an interrogator to monitor the wavelength shift. In spite of this, the present work will focus on analysing these configurations, since they are more reliable in terms of noise and present a high versatility when using different optical configurations that optimize the sensor performance.

However, precisely due to the many existing contributions dealing with different procedures to obtain wavelength-based optical fibre biosensors, there is a need to synthesize the main parameters that indicate the quality of the main optical biosensor platforms used nowadays. In this respect, a selection of the most relevant contributions offering an "all-in-one" solution in terms of simple fabrication, sensitivity, resolution and limit of detection (LOD) is done in this work. For this purpose, the second part of the manuscript will introduce the latest trends in wavelength-based techniques used when developing optical fibre biosensing platforms, with a brief theoretical explanation of their working principles. Then, the third section will classify and compare these sets of sensors on the basis of several parameters analysed. Finally, some conclusions will be extracted on the optimum way to develop such kind of biosensors, as well as an outlook to the future research lines that can be taken into account to address this topic.

2. Wavelength-based optical fibre sensing platforms

Three different groups of wavelength-based optical fibre sensing platforms can be observed in Fig. 3. The first one involves any kind of sensor based on generating a Bragg grating inside its core: short/long fibre Bragg gratings (FBGs and LPFGs) and tilted FBGs (TFBGs). A second group consists of all kind of interferometers, either fabricated by fusing different types of fibres (they will be called "all fibre") or based on a Fabry–Pérot (FP) cavity on the tip of an optical fibre. This last group will consider FP interferometers made by fusing optical fibres or by depositing a thin-film on the fibre tip to form nanoFabry–Pérot interferometers (NFPs). Finally, the third group joins those platforms based on the deposition of a thin-film onto the optical fibre substrate in order to generate resonances.

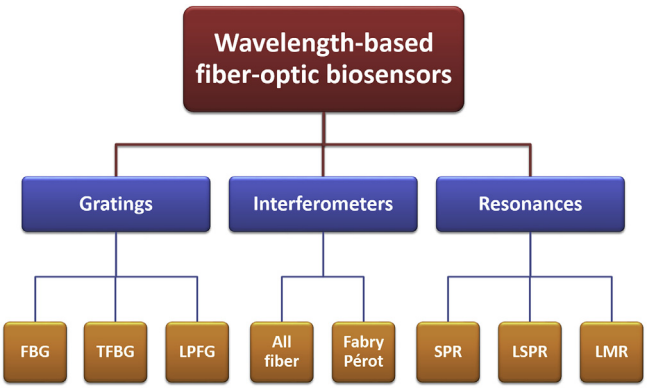

Fig. 3. Conceptual map of the wavelength-based optical fibre biosensing platforms analysed in this contribution.

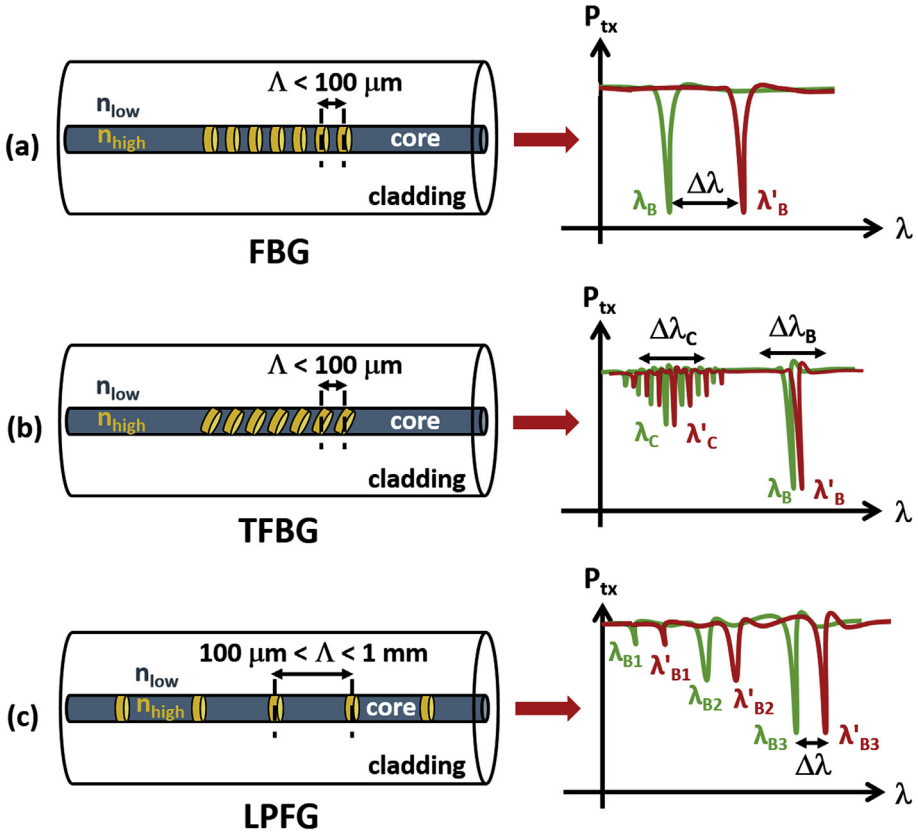

Fig. 4. Schematic representation of the fibre Bragg grating-based structures analysed and their corresponding spectral response. (a) Simple FBG, (b) tilted FBG and (c) LPFG.

2.1. Optical fibre sensors based on gratings

2.1.1. Fibre Bragg gratings

Fibre Bragg gratings are single-mode fibres where a periodic perturbation of the core refractive index has been practised (n_{low} - n_{high}), as shown in Fig. 4. Depending on the grating period generated inside the fibres, optical fibre sensors based on gratings can be divided into short-period fibre Bragg gratings (FBGs) and long-period fibre Bragg gratings (LPFGs). For FBGs, the periodicity of the grating structure is typically below 100 μm, whereas for LPFGs the periodicity ranges from 100 μm to 1 mm. This classification obeys the fact that, depending on the grating period, there is a coupling to copropagating and counter-propagating modes at specific wavelengths (Erdogan, 2000).

In the case of FBGs (Fig. 4a), the short period allows a coupling from the core mode to the counterpropagating core mode. This coupling is translated into a quite sharp attenuation band of just a few picometers wide obtained in the optical spectrum at λ_B, as shown in expression 1:

$$\lambda_B = 2n_c^{eff}\Lambda \quad (1)$$

where n_c^{eff} is the effective index of the fibre core mode and Λ the period of the refractive index variation along the FBG.

Regarding the typical applications of FBGs, they can sense temperature (Zhou et al., 2018), strain (Rodriguez-Cobo et al., 2014) or torsion (Budinski and Donlagic, 2017), important variables to be controlled in biosensing applications. However, FBGs are not sensitive to the surrounding refractive index (SRI), a key element in an optical fibre biosensor, because its cladding diameter is typically 125 μm. Consequently, the core is too far separated from the external medium, so those changes occurring outside cannot affect the effective index of the core mode. Indeed, only by reducing the FBG diameter (i.e. by an etching process) is it possible to obtain a refractometer (Liang et al., 2005). In order to keep on improving the SRI sensitivity, a thin-film can be deposited onto the etched structure, leading to an increase in the effective indices of the modes propagating inside the new waveguide (Luo et al., 2017).

2.1.2. Tilted Fibre Bragg gratings

A special mention is deserved by those FBGs where the periodic variation of the core refractive index is induced by tilting the grooves of the fabrication mask by an angle θ with respect to the propagation axis. This makes it possible to obtain tilted FBGs (TFBGs) (Laffont and Ferdinand, 2001). Unlike original FBGs, where the bands corresponding to coupling to counterpropagating cladding modes are negligible compared to the band coupling to the counterpropagating core mode, the fact of tilting the grooves in a TFBG also makes it possible to visualize the bands coupling to different counterpropagating cladding modes (see Fig. 4b). In addition, in TFBGs the Bragg condition given in expression 1 has to be rewritten taking into account the resonance wavelength λ_{rm} of each *m*-th cladding mode, as indicated in expression 2 (Albert et al., 2013):

$$\lambda_{rm} = (n_{core}^{eff} + n_{clad-m}^{eff})\frac{\Lambda}{cos\theta} \quad (2)$$

where θ is the tilt angle of the grating and n_{clad-m}^{eff} is the effective refractive index of the *m*-th cladding mode. The plus sign indicates the addition of the counterpropagation of the cladding modes obtained after tilting. It is simple to observe that by setting $\theta = 0$ and when a coupling to the counterpropagating core mode is performed, expression 2 turns into expression 1.

The fact of owning bands that can be coupled to cladding modes makes this optical structure sensitive to SRI changes, since the effective indices of cladding modes depend on the SRI. By monitoring the changes of the cladding mode effective index, an accurate measurement of the external refractive index can be obtained (Chan et al., 2007;

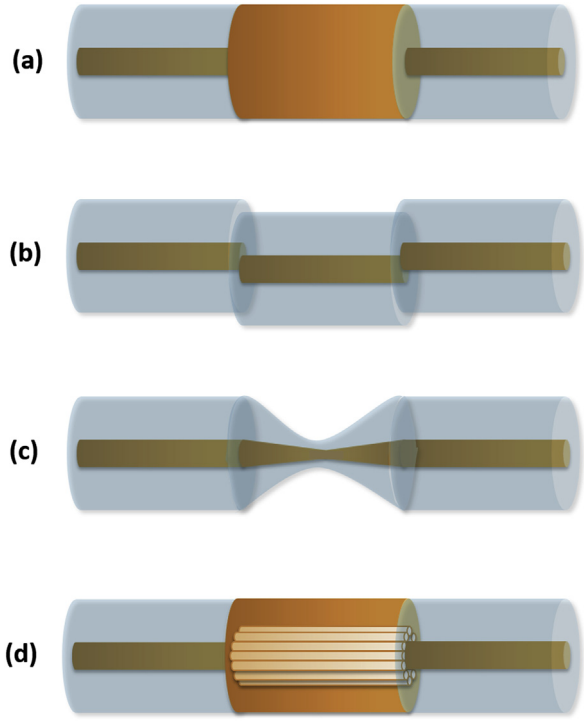

Fig. 5. Schematic representation of optical fibre-based interferometers varying (a) the core diameter, (b) the alignment, (c) the shape and (d) the type of the fibres.

Caucheteur and Mégret, 2005). Moreover, in (Zhou et al., 2017), the development of an absolute refractive index sensor based on a TFBG is proved. In addition, by accessing the propagation of the higher order cladding modes, the capability of TFBGs to detect SRI changes is enhanced (Chen et al., 2005).

Also, increasing the tilt angle of a TFBG makes it possible to obtain structures based on coupling to copropagating modes, as occurs in long period gratings (Luo et al., 2018, 2016; Zhou et al., 2006), the device presented in the next section. Moreover, highly tilted FBGs are inherently very sensitive to the surrounding medium's refractive index, but with temperature sensitivities of 4–7 p.m./°C in the C-L band. This result is significantly lower than those of the LPFGs and FBGs and is, of course, interesting when designing biosensors. Finally, it is always possible to keep increasing this sensitivity, either by mismatching the cores of the input fibre and the TFBG segment (Guo et al., 2009) or by depositing thin-films that gently enhance the effective indices of the cladding modes propagating inside the fibre (Jiang et al., 2015). Therefore, there are several degrees of freedom to enhance the possibility of detecting changes in the outermost medium without greatly compromising the spectral width of the dips generated. In this sense, TFBGs are potentially good platforms for detecting chemical and biochemical species.

2.1.3. Long-period fibre gratings

LPFGs present a longer periodicity between refractive index variations within the core, which allows a coupling to be obtained between the core mode and the copropagating cladding modes (Erdogan, 1997). As a result, several dips can be observed in the transmission spectrum (see Fig. 4c), whose location is ruled by expression 3 (Anemogiannis et al., 2003; James and Tatam, 2003):

$$\lambda_{rm} = (n_{core}^{eff} - n_{clad-m}^{eff})\,\Lambda \tag{3}$$

where n_{core}^{eff} is the effective refractive index of the propagating core mode, n_{clad-m}^{eff} is the refractive index of the m-th cladding mode, and Λ is the period of the LPFG.

In LPFGs, as in TFBGs, there is a dependence of the resonance wavelength on the cladding modes (see expression 3) and, consequently, on the SRI. A maximum sensitivity can be attained by combining three phenomena. First, the turn-around point or dispersion turning point (TAP/DTP) (Shu et al., 1999), a region where the slope of one or several phase matching curves extracted from expression 3 reaches a maximum value. Second, the mode transition (MT) (Cusano et al., 2006; Del Villar et al., 2005), a phenomenon that can be observed when a high refractive index coating is deposited on the cladding of the LPFG. Finally, the third is a combination of MT, DTP (this leads to sensitivities of circa 10000 nm/RIU in the water region (Pilla et al., 2012)) and cladding etching (Chen et al., 2007). This combination can lead theoretically to more than 100000 nm/RIU in water (Del Villar, 2015) and experimentally to values approaching this record sensitivity (Śmietana et al., 2016).

2.2. Optical fibre sensors based on interferometry

An optical interferometer is a phase-modulation device based on the superposition of several modes propagating inside an optical waveguide (Boudoux, 2017). Such waveguide is designed so that the input light is propagated through two or more optical paths and then recombined at the output. After the recombination, all paths converge, but those modes propagating through different paths experience a different phase shift. This induces attenuation and transmission bands in the optical spectrum. Considering two monochromatic waves overlapping spatially and applying the principle of superposition of waves, the general solution for the intensity of an interferometer is shown in expression 4 (Boudoux, 2017):

$$I = I_1 + I_2 + 2\sqrt{I_1 I_2}\cdot cos(\phi) \tag{4}$$

where I_1 and I_2 are the intensities of each of the original monochromatic waves and $\phi = \phi_1 - \phi_2$ is the phase delay between those original waves. This is the working principle of every basic interferometer. Some strategies will be presented in the next subsections in order to obtain simple fibre interferometric structures.

2.2.1. All-fibre interferometers

As previously suggested, all-fibre interferometers refer to a class of interferometers made by fusing fibres or fibre segments. A first simple example of this structure can be obtained by splicing two standard multimode or monomode optical fibre pigtails to a coreless fibre segment (Fig. 5a). In such structures, light in the input fibre couples to several modes within the intermediate fibre and recouples in the output fibre. As a result, several transmission and attenuation bands are created in the resulting optical spectrum, corresponding to constructive and destructive interferences in the intermediate fibre. Single-mode – multimode – single-mode (SMS) structure (Silva et al., 2012; Socorro et al., 2014a) is an example of such interferometers, as well as its corresponding etched, polished and/or thin-film deposited versions for improving their sensitivity to SRI (Cardona-Maya et al., 2017; Socorro et al., 2014a; Wu et al., 2011). The same occurs when using multimode – coreless – multimode (MCM) structures (Jung et al., 2006).

A second way to obtain all-fibre interferometers is by inducing misalignments (Fig. 5b). Here, the cylindrical symmetry of the optical fibre is broken. Consequently, there are mode beatings provoking interferometry inside the waveguide and, thus, attenuation and transmission bands that can be used for sensing (Luna-Moreno et al., 2007; Villatoro and Monzón-Hernández, 2006). Other strategies change the shape of the intermediate optical fibre segment between the input and output pigtails. This is the case of non-adiabatic tapers (see Fig. 5c) (Yadav et al., 2014), which can be used for generating a spectral interferometry pattern that can be conveniently modulated in order to obtain narrow resonant bands for detection. There is also the possibility of repeating the same interferometric pattern several times along the

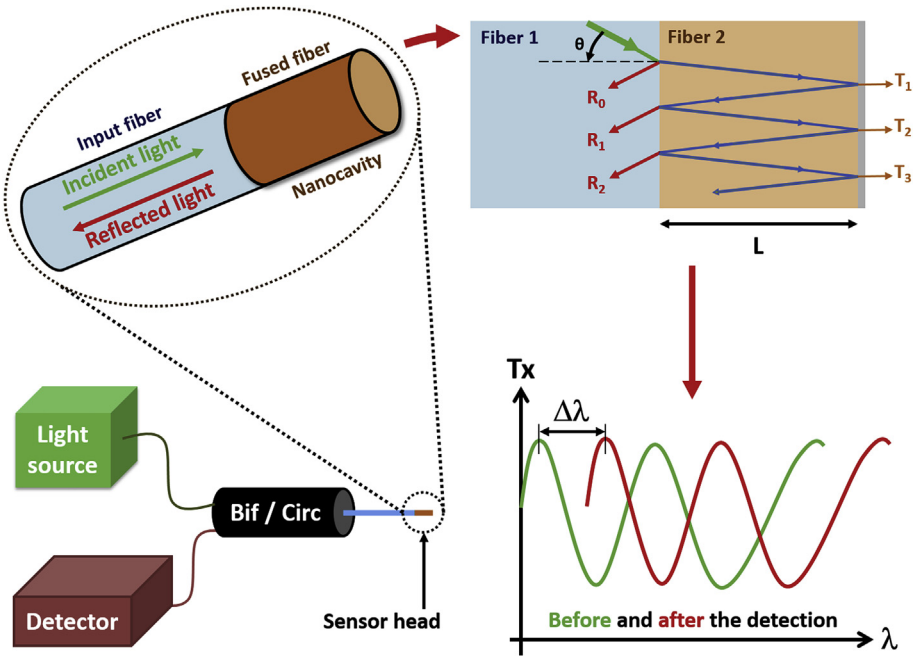

Fig. 6. Schematic of a typical experimental set-up for either a Fabry–Pérot or a nanoFabry–Pérot based optical fibre interferometer (FPI), together with the internal reflections and an obtained spectrum before and after detection. The addition of layers, particularly when detecting bioreceptor–analyte complexes, induces a red-shift in wavelength.

sensing area (Xiong et al., 2014), or fusing specialty fibres such as suspended core (Lopez-Torres et al., 2018), photonic crystal (Dash et al., 2015) or hollow core fibres (Abdallah, 2018) (see Fig. 5d).

All the previous structures present different geometries and types of splicing in order to change the propagation symmetry inside the fibre. This excites higher order modes that interact with the surrounding medium, giving the possibility to subtract more or less optical power to the original propagation modes, as occurs in Mach–Zehnder interferometry (MZI). The numerous recent contributions reporting the generation of all kinds of MZIs inside a single fibre structure have baptized the state-of-the-art as '*in-fibre MZI*' (Zhao et al., 2019).

2.2.2. Fabry–Pérot and nanoFabry–Pérot interferometers

This group of interferometers uses a reflective set-up whose schematic is reflected in Fig. 6 (Islam et al., 2014). An FPI sensor consists of a cavity between at least one semi-reflective surface and another either semi-reflective or fully-reflective surface. Both surfaces create two reflected paths that allow the interference of the light modes between them. In this way, the reflected power obtained at the detector is determined analytically by expression 5:

$$P_r = P_i \cdot (R_1 + R_2 - 2\sqrt{R_1 R_2} \cdot \cos(\phi_{FPI})) \quad (5)$$

where P_i and P_r are the incident and reflected optical powers, respectively, and R_1 and R_2 are the reflection coefficients in the surfaces. ϕ is the phase shift between reflective surfaces (for instance, between points T_1 and T_2 in Fig. 6) and, according to expression 6:

$$\phi_{FPI} = \frac{4\pi n L}{\lambda} \quad (6)$$

where L is the distance between interfaces, λ is the operational wavelength and n is the refractive index of the medium between interfaces of the Fabry–Pérot cavity (Islam et al., 2014). Also, FPIs can be divided into extrinsic or intrinsic sensors, depending on whether the interferometry is done externally (Chen et al., 2010; Poeggel et al., 2015) or the own structure generates an internal interferometry (Domingues et al., 2018; Wang et al., 2018). In both cases, the goal is to obtain peaks based on varying either the length of the interferometry or the refractive index of the reflecting interfaces.

Another way of obtaining similar results is by generating nanoFabry–Pérot interferometers (nFPIs). The fact of depositing a thin-film of determined materials on the tip of an optical fibre creates the necessary conditions to induce light reflections inside the nanocavity so that an interferometer is constructed. In this respect, either FPIs or nFPIs are interesting alternatives when designing medical devices, since their reduced size and reflective configuration permits their introduction in ferrules or catheters inside the body (Hernández-Romano et al., 2016; Wallner et al., 2013) or even testing microtiter plates such as those used in ELISAs.

As occurs in Bragg gratings, optical fibre-based interferometers are widely reported for biosensing since they can provide a low-cost platform with well-defined bandwidths due to the mode beatings inside the sensing area. Their sensitivity is not so high in comparison to grating-based sensors. However, strategies such as including microcavities, reducing the diameter of the interferometric cavity or depositing thin-films of higher refractive index than that of the optical waveguide (Cardona-Maya et al., 2017) can help enhance it.

2.3. Optical fibre sensors based on resonances

Inside a standard optical fibre, the core mode transmits light mostly confined within the core (the guided field), and some part is transmitted through the cladding (the evanescent field). The penetration depth (d_p) of this evanescent wave is a key parameter when sensing. It is defined as the distance from the interface at which the amplitude of the electric field is decreased by a $1/e$ factor (Gouveia et al., 2013). Following the approximation of geometrical optics, this can be expressed as indicated in expression 7 (Leung et al., 2012):

$$d_p = \frac{\lambda}{2\pi\sqrt{n_{core}^2 sin^2(\theta) - n_{clad}^2}} \quad (7)$$

where n_{core} and n_{clad} are the core and cladding refractive indices respectively, θ the incidence angle at the core-cladding interface and λ the incidence wavelength.

The penetration depth is crucial in terms of evaluating the interaction of light with the medium surrounding the optical fibre and it can be modulated by thin-films or nanostructures deposited onto the fibre. Moreover, depending on the parameters of the waveguide, the thin-film and the surrounding medium, it is possible to generate attenuation bands at certain wavelength ranges (i.e. resonances), as shown in Fig. 7.

Three types of resonances can be distinguished: long-range surface

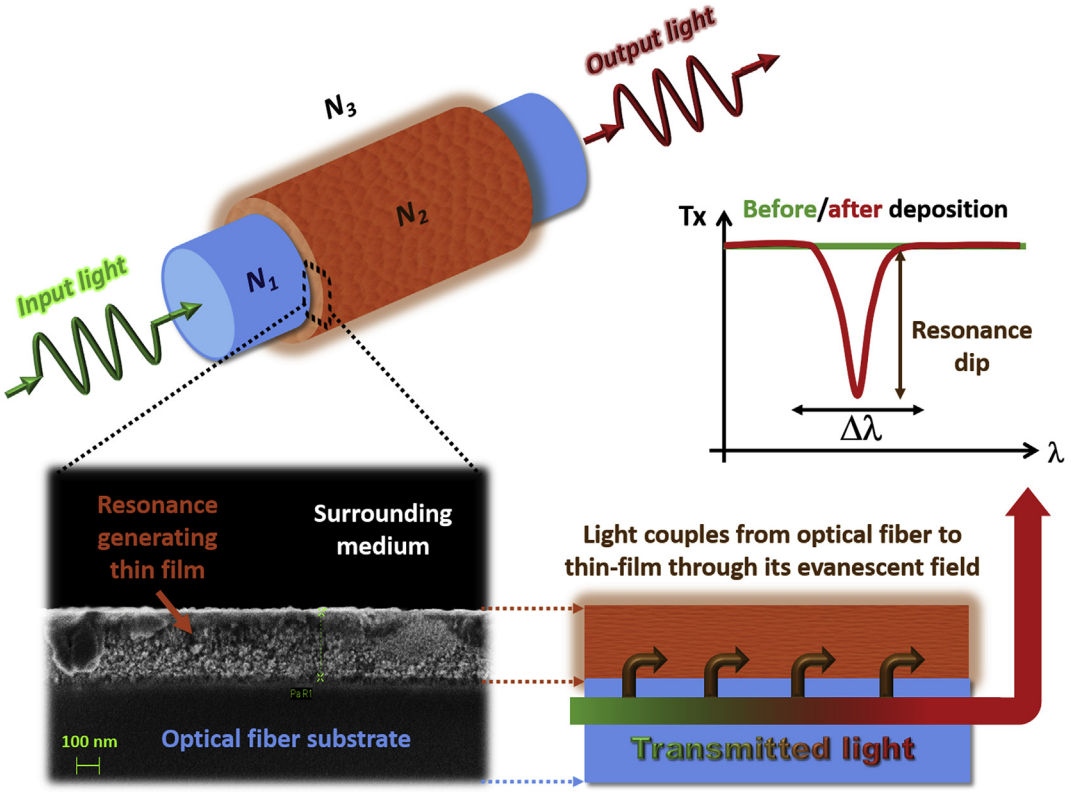

Fig. 7. Schematic representation of the working principle of an optical resonance generated onto an optical fibre where a thin-film has been deposited. It can be observed how the thin-film causes the incident light to couple light modes inside it to generate the corresponding resonance. If the light mode is coupled to a surface plasmon, the obtained resonance will be an SPR, whereas if there are subsequent light modes that are coupled inside the thin-film, a lossy mode resonance (LMR) will be obtained.

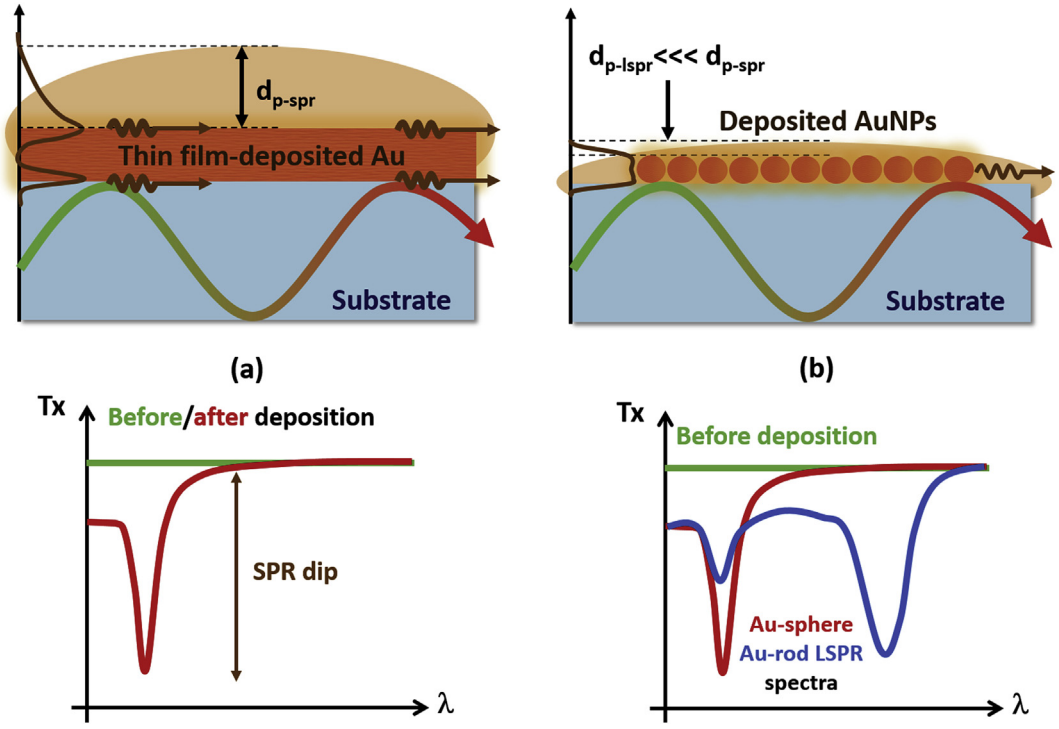

Fig. 8. Schematic comparison between (a) SPRs and (b) LSPRs generation after depositing either a gold thin-film or gold nanoparticles onto the fibre, with their corresponding spectra. In (b), depending on the aspect ratio of the gold nanoparticles, more than one LSPR can be generated with enhanced sensitivity as a function of the SRI. The red spectrum is typical of nanospheres, whereas the blue spectrum indicates the presence of different shapes (nanorods, for instance).

exciton-polaritons (LRSEPs) (Zhang, 2011), surface plasmon resonances (SPRs) (Špačkova et al., 2016), and lossy mode resonances (LMRs) (Del Villar et al., 2017a,b; Wang and Zhao, 2018). LRSEPs are still under basic research, though some advances are being made in this area. Given the more advanced state of the art in SPRs and LMRs, this contribution will focus on SPRs and LMRs henceforward.

2.3.1. Surface plasmon resonances (SPRs)

As is well known, an SPR is a resonance that occurs when depositing a metallic thin-film (typically gold or silver) on a dielectric waveguide. Metals are suitable for SPR generation because the real part of the deposited thin-film permittivity is negative and higher in magnitude than both its own imaginary part and the permittivity of the material surrounding the thin-film (Yang and Sambles, 1997). Under these conditions, there is a charge density wave associated with an electromagnetic field which reaches its maxima at the metal–dielectric interface and then decays evanescently into both media (Homola et al., 1999). This charge density wave is called a surface plasmon polariton (SPP) and it is generated within the penetration depth of the optical substrate as a transverse magnetic (TM) wave. Consequently, SPPs are typically excited with TM polarized light. These SPPs propagate with a wave vector (k_{SP}) related to the dielectric constants of both the dielectric and the metallic film. On the other hand, the evanescent field of the light guided in the substrate propagates with a wave vector k_{EV} by means of total internal reflection (TIR) in a direction parallel to the light propagation. The only way to produce an SPR is to equal k_{SP} to k_{EV}, since then is when the SPP can be excited by the evanescent wave and thus obtain the SPR. This is known as the "phase-matching" condition. In this respect, there is a determined range of excitation angles where the SPR shows up and can be used for sensing purposes. When this happens, the intensity of the reflected light decreases and the spectrum shows an attenuation band at those angles where the SPR can be excited (Tang et al., 2010). This set of angles can be achieved using the Kretschmann configuration (Liedberg et al., 1995), and the same resonance phenomenon can be observed by fixing the angle of incidence and analysing a range of wavelengths (see Fig. 8a).

In optical fibres, the process of exciting an SPP is quite similar to the Kretschmann configuration, but presents some particularities. First, the light is guided by the optical fibre, so it is not possible to control the incidence angle. Moreover, the numerical aperture of the fibre strongly limits the range of incidence angles that meet the SPR generation condition. Consequently, tracking the wavelength shift of the resonance in the optical spectrum is the basis of the detection. Apart from this, SPPs are obtained when TM polarized light is transmitted. However, the cylindrical symmetry of the fibre is not prepared to maintain a polarization state (Zubiate et al., 2015). Therefore, there is a need to use either a polarization maintaining fibre or a system based on an in-line polarizer and a polarization controller, with the corresponding increase in the final cost of the device. In general, the SPRs generated in optical fibre sensors are not as sensitive as SPRs in Kretschmann configuration, where sensitivities of 57000 nm/RIU are achieved (Radan and Homola, 2006).

2.3.2. Localized surface plasmon resonances (LSPRs)

LSPRs have demonstrated enhanced properties with respect to SPRs, which typically use planar gold thin-films. The reason for calling these resonances "*localized*" is the fact of being generated in metal nanoparticles and, therefore, localizing the phenomenon in a reduced space limited to the own nanoparticle (see Fig. 8b). This allows a confinement of the SPP in a space comparable to or smaller than the wavelength of light used to excite the SPP (Rycenga et al., 2011).

Two important effects can be extracted from this phenomenon. They are shown in Fig. 9. First, the electric field in the proximity of the particle's surface is strongly enhanced and, unlike thin-film-generated SPRs, the LSPR presents a non-linear dependency on the nanocoating thickness (Jatschka et al., 2016). As a result, the second effect in LSPRs is that the electric field intensity drops more strongly with the distance from the surface than in SPRs. Consequently, the penetration depth in LSPRs is much lower than in SPRs. A greater penetration depth in SPRs can be good in terms of sensitivity to SRI variations as a whole, but at the same time it is also possible to detect other variables such as temperature or refractive index and other external changes that interfere with the analytes and can be considered as noise (Jatschka et al., 2016). Consequently, LSPRs are more resistant to these effects.

Finally, LSPRs are more versatile than SPRs when generating resonances. For instance, a spherical nanoparticle normally shows a single absorption band, whose central wavelength depends on the nanoparticle size. However, a non-spherical nanoparticle can present different absorption bands according to its shape (see Fig. 8b). Thus, gold nanorods usually present two absorption bands: one normally centred near 520 nm and the other varying in wavelength according to its aspect ratio (the quotient between the longitudinal and transversal dimensions of the rod). The second absorption band is more sensitive to the surrounding medium changes, so it can be used to develop LSPR-based biosensors with enhanced sensitivity (Pérez-Juste et al., 2005; Rycenga et al., 2011; Yuan et al., 2016).

2.3.3. Lossy mode resonances (LMRs)

Lossy mode resonances (LMRs), also named by some authors as guided mode resonances (Yang and Sambles, 1997), are based on the generation of lossy modes in a waveguide with a lossy cladding (Batchman and McWright, 1982; Marciniak et al., 1993). Unlike SPPs, lossy modes (LMs) are generated when the real part of the thin-film permittivity is positive and higher in magnitude than both its own imaginary part and the permittivity of the material surrounding the thin-film (Yang and Sambles, 1997). Under these conditions, LMRs are induced when a mode guided in the substrate experiences a transition to guidance in the thin-film. This causes a reorganization of the effective indices of the rest of the modes guided in the substrate at the same time as their evanescent field is increased (Corres et al., 2015). Consequently, transmission losses are increased, which can be observed in the form of several dips in the transmission spectrum that are red-shifted as a function of the coating thickness (see Fig. 10).

Many materials other than pure metals (typical of SPRs) can induce LMRs. Thus, several contributions have reported generating LMRs with metal oxides (Andreev et al., 2005; Śmietana et al., 2018), polymer coatings (Del Villar et al., 2012; Zamarreño et al., 2011), two-layer-coated structures combining both materials (Zamarreño et al., 2010) or even immunosensors consisting of multilayers of polymers and antibodies (Socorro et al., 2014b, 2012).

Two relevant reviews on the topic have already been published (Del Villar et al., 2017a,b; Usha et al., 2018) and a thorough analysis on the rules for optimizing the performance of LMR-based sensors can be found (Del Villar et al., 2012), where two basic rules are given: the first LMR is the most sensitive one. Unlike in SPRs, several resonances can be obtained and their position in the optical spectrum is controlled by means of the coating thickness. As a result, the sensitivity of the device increases as the refractive index of the thin-film increases and as the SRI approaches that of the substrate (Del Villar et al., 2012). In addition, LMRs can be obtained with both TE and TM polarized light. Consequently, it is possible to avoid the use of a polarizing system (Del Villar et al., 2012, 2010; Zamarreño et al., 2011), although it is true that polarizing the light involves selecting only its TE or TM component and the bandwidth of the obtained resonance is reduced (Del Villar et al., 2017a,b). This has made it possible, in the case of thin-film coated D-shaped fibre, to convert this optical platform into a good candidate for biosensing (Del Villar et al., 2017a,b; Zubiate et al., 2017).

Several contributions have shown a comparison between the application of nanoparticles or thin films to generate LMRs for different sensing purposes (Mishra et al., 2016; Usha et al., 2015a,b), but perhaps the most interesting publication consisted in comparing an SPR with an LMR, showing that a better sensitivity is obtained in the case of the LMR

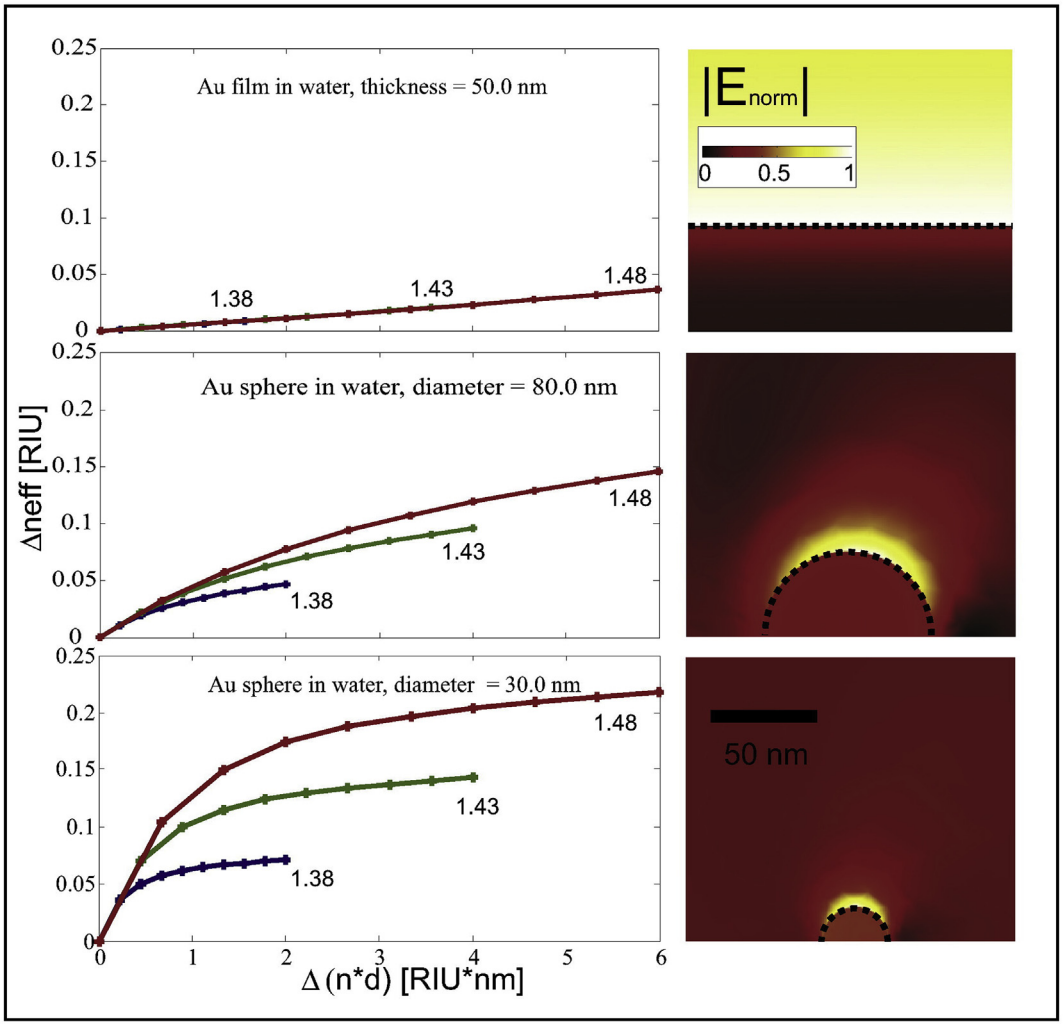

Fig. 9. Numerical SPR comparison among several circumstances involving the deposition of planar gold thin-film (top), 40 nm-radius (medium) and 15 nm-radius (bottom) embedded gold nanoparticles. Right – normalized electric field values, where the location of the maximum values depending on the gold thin-film can be observed. Left – non-linear effect visible of the proximity of the nanoparticles with respect to the response of a planar gold thin-film. Reproduced with permission of Elsevier (Jatschka et al., 2016) with Creative Commons Attribution License (CC BY 4.0).

(Usha et al., 2015a,b). Finally, it has been proved that it is possible to obtain both LSPRs and LMRs with the same device, using the LSPR as a reference for tracking the LMR shift as the sensitive thin-film reacts (Rivero et al., 2016, 2013). For this purpose, the corresponding LSPR-generating nanoparticles are embedded in a matrix before depositing the optical fibre.

3. Optical parameters analysed

When designing biosensors, there are some generic parameters such

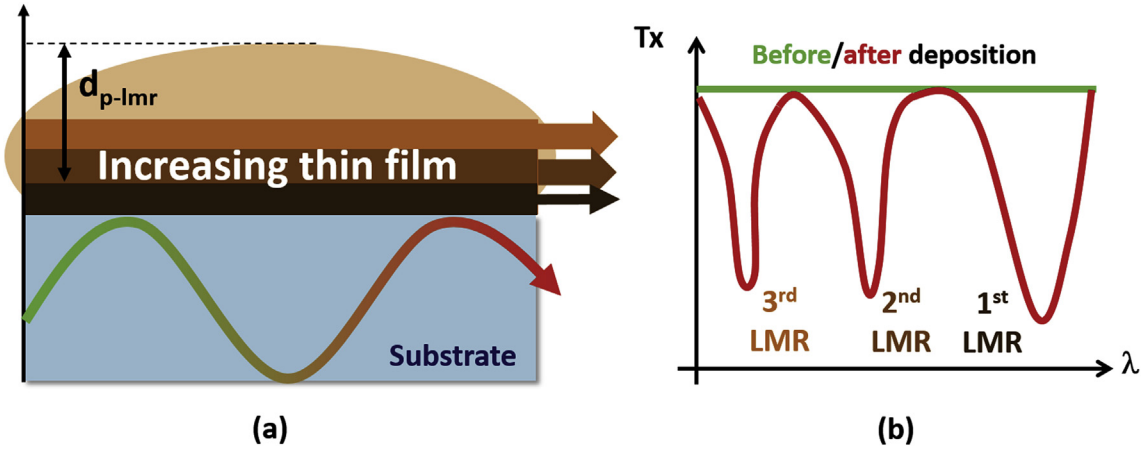

Fig. 10. (a) Schematic representation of the LMRs formation with the corresponding spectrum as a function of the increasing thin-film thickness.

as uncertainty, accuracy, precision or response time to be taken into account when designing and, overall, calibrating them. However, these parameters strongly depend on the measurement method, the configuration set-up, the materials deposited as thin-films (if used) and even on how good the instrumentation is. Additionally, capabilities such as cross-sensitivity or selectivity depend on the affinity between the biomarker and the bioreceptor, as well as the actual conditions in which the experiment is being carried out. For instance, experiments can be done under controlled buffer conditions, or in more complex matrices such as blood serum, plasma or blood itself. As the complexity of the testing matrix increases, so does the potential number of difficulties that it is necessary to handle, since there are many other molecules that can interfere with the detection of the analyte. Finally, parameters like regeneration, repeatability or reproducibility also depend on the experimental kit and, therefore, on the possibility of introducing external agents, like enzymes, that can unbind the already created bioreceptor–biomarker bonds to start the detection process again (Chiavaioli et al., 2017).

In view of the previous issues, the focus will be centred on those parameters that lead to a more objective evaluation of an optical sensing platform. These parameters are provided in most of the articles published on optical fibre biosensors and they are the sensitivity to the surrounding refractive index (SRI), the spectral bandwidth and, finally, as a derived magnitude of the previous two, the Figure of Merit (FOM). In order to contrast the adequateness of these parameters in terms of evaluating the performance of an optical fibre biosensor, their relationship with the limit of detection (LOD) will be analysed.

3.1. Sensitivity

The sensitivity is the ratio of the wavelength shift experienced by the resonance wavelength of the transmission or attenuation band as the SRI changes:

$$S = \frac{\Delta\lambda}{\Delta n} \tag{8}$$

It must be pointed out that the biomarker–bioreceptor interaction is basically the adhesion of thin-film progressively deposited over the bioreceptor layer and, consequently, the wavelength shift is due to variations of the refractive index and thickness of the material surrounding the waveguide. Consequently, another good parameter could also be the sensitivity to thickness changes in the coating. However, this parameterization will also depend on the refractive index of the material selected for testing this sensitivity. By contrast, the sensitivity to the refractive index, though not an exact prediction of the further performance of the biosensor, is easier to obtain and is independent from additional variables. Therefore, the sensitivity to the SRI is a reference value for assessing the biosensor before using it for detecting a specific analyte (Chiavaioli et al., 2017).

3.2. Full width at half maximum/minimum (FWHM) and Q-factor

The central wavelength of a transmission or attenuation band is the wavelength location of the maximum or minimum value of that band. This central wavelength, also called the resonance wavelength, will be named λ_0 henceforward.

Once λ_0 has been defined, the full width at half minimum or maximum (FWHM) is the wavelength range covered by the resonant band at a level 3 dB above/below its minimum/maximum, depending on whether the measurements are in transmission or in absorption (Socorro et al., 2014b).

Another parameter closely related to the FWHM is the quality factor (Q-factor), which is basically the quotient between λ_0 and the FWHM:

$$Q = \frac{\lambda_0}{FWHM} \tag{9}$$

A high Q value indicates that its FWHM is small in comparison with its central wavelength, which denotes a good capability of distinguishing between similar SRI values. Therefore, the Q-factor is a good indicator of the resolution of the measurements, together with the resolution of the detector. Moreover, since Q is a relative measurement, the effect of dealing with a higher or lower λ_0 is minimized.

3.3. Figure of merit (FOM)

After defining the sensitivity and FWHM, the Figure of Merit can be calculated as the quotient between these two, as indicated in expression 10. It is normally expressed in RIU^{-1}.

$$FOM = \frac{S}{FWHM} \tag{10}$$

This value is an idea of how much the sensor is approaching the ideal situation (i.e. the highest sensitivity and the lowest FWHM). Though it is true that the FOM is obtained as a function of the SRI, in the biosensors field the wavelength shifts are due to the analyte–bioreceptor recognition. A strategy that may simulate this behaviour is to obtain the FOM as a function of thickness, but as stated for the sensitivity, it is easier to operate with the SRI.

3.4. Limit of detection (LOD))

The LOD is one of the main parameters analysed when addressing the design and characterization of biosensors. It indicates the hypothetical minimum value of the analyte concentration that the sensor is capable of detecting under ideal experimental conditions. There are three main criteria to calculate the LOD (Chiavaioli et al., 2017). The first method is based on the use of the standard deviations at low concentration. After taking up to 10 measurements of both the blank sample (before taking actual measurements) and several discrete concentrations between 1 and 5 times the suspected LOD, the standard deviation σ_y is calculated. After that, expression 11 can be used to obtain the experimental LOD:

$$y_{LOD} = \bar{y}_{blank} + t_{\alpha,k-1}\sigma_y \tag{11}$$

where $t_{\alpha,k-1}\sigma_y$ is the α-quantile of the t-Student function with $k-1$ degrees of freedom at $(1-\alpha)$ confidence interval. The second approach is based on the use of the calibration curve of the biosensor and on recommendations by the IUPAC. According to this method, the LOD can be obtained by performing expression 12:

$$y_{LOD} = f^{-1}(\bar{y}_{blank} + 3\sigma_{max}) \tag{12}$$

which stands for the inverse of the fitting function (typically a sigmoidal curve) evaluated in the point $(\overline{y}_{blank} + 3\sigma_{max})$, which means $\bar{y}_{blank}$ plus three times the maximum standard deviation obtained among all the measurements. Finally, the third strategy is to calculate the quotient in expression 13:

$$y_{LOD} = \frac{R}{S_{surf}} = \frac{R}{\Delta n/\rho_{max}} \tag{13}$$

where R is the sensor resolution and S_{surf} is the quotient between the RI change (Δn) and the maximum surface density concentration (ρ_{max}) of the target analyte. Given the fact that there are no ideal or absolute measurements and even more so when talking about the bio disciplines, it seems that the best way to determine LOD is the first or the second one, although the third approach is common for SPR-based biosensors (Chiavaioli et al., 2017). Both of them are statistically calculated, which gives added value to the investigations. The second offers an approximation based on IUPAC standards, which means that it may be more rigorous from a scientific point of view and it is globally accepted.

As shown, a good calculation of the LOD needs a statistical analysis and it depends on many characteristics such as the affinity between the bioreceptor and the analyte. Therefore, it is important to take a look at

those parameters that can be used for determining the performance of the device independently of the conditions that affect the LOD. This is the aim of the next section: to compare the different optical structures with parameters such as the FOM, the Q-factor and the sensitivity, which will be the basis for the assessment of the different types of biosensors found in the literature.

4. Assessment of latest trends in optical fibre wavelength-based biosensors

Monitoring the change of a biomarker in real time allows the identification of the susceptibility to different therapies and interactive optimization of medical treatments with reduced time and costs, compared to clinical validation of therapies (Liang et al., 2017). Different protein biomarkers are correlated with the presence of pathogenic processes and diseases. Usually, the performance of a new optical fibre biosensor is evaluated by direct binding model assays. According to the reviewed literature, the most standardized biological measurements involving the detection of bioreceptor–analyte complexes are IgG/*anti*-IgG, (strept)avidin/biotin and BSA/*anti*-BSA. They are normally chosen because of their low purchase price, ease of handling, availability and widely studied binding and immobilization process. Once adequate performance of the biosensor is proved, the biomarkers associated with specific pathologies are employed in order to identify a specific use for the biosensor.

This section summarizes the results achieved in the literature using wavelength-based optical fibre biosensors. The publications have been selected and analysed considering the parameters described in section 3, in order to see if the optical structure determines the values obtained for each of the studied parameters. All these data are collected in Tables 1–4, corresponding to the different optical platforms described in section 2 (there were some references where no information on some of the parameters was given. This especially affected TFBG-based sensors, where in some cases the amplitude of the resonant peaks envelope is used for sensing instead of the wavelength shift).

4.1. Optical fibre biosensors based on gratings

According to section 2, TFBG-based sensors should be one of the structures that provide the best performance in the domain of biosensors. In addition, TFBGs are combined with other phenomena in order to improve their performance. A good example is the deposition of gold thin-films, which increase the inherent sensitivity of the TFBG by means of an SPR. In this respect, TFBG-SPR sensors have been recently developed for many bio-sensing applications, such as the detection of Newcastle virus (Luo et al., 2018) or porcine circovirus type 2 (PCV2) (Luo et al., 2016) and to detect different cancer biomarkers like cytokeratin 7 and 17 (Ribaut et al., 2017, 2016), urinary proteins (Guo et al., 2016), breast cancer biomarker (Sun et al., 2017), thyroglobulin (Quero et al., 2016), etc. The optical platforms employed to detect cytokeratin 7 and 17 achieved the best Q-factors: Q- 7712 (Ribaut et al., 2016) and Q- 5142 (Ribaut et al., 2017) respectively.

Another technique that has been applied to TFBG-SPRs consists of an interrogation with circularly polarized light to the optical fibre surface, which maximizes the optical coupling with the SPR. This method allowed Q values of 15600 to be obtained in a work where streptavidin and human transferrin were detected (Voisin et al., 2014). The FOM of this work was around 5000 RIU^{-1}, the best FOM achieved so far with a wavelength-based optical fibre biosensor (see Fig. 11).

Following the same principle, TFBGs can excite localized surface plasmon resonances (LSPR) when gold nanoparticles are used instead of gold thin-films (Bialiayeu et al., 2011). As a proof of concept, an analysis of TFBGs modified with several types of gold nanoparticles for protein detection was performed by Lepinay et al. (2014), which led to an increased Q-factor of 15000. In these conditions, the LOD for biotin decreased from 21.99 ng/ml without nanoparticles to 1.95 pg/ml with

Table 1
Analysed parameters for TFBG-based optical fiber biosensors.

Substrate	Biomarker	λ_0 (nm)	FWHM (nm)	Q-factor	Sensitivity (nm/RIU)	RIU range	FOM (RIU^{-1})	Limit of detection	Reference
10° TFBG-SPR coated with Au film	Glycoprotein: concanavalin A	1545	0.22	~7000	576	1.32–1.35	2618	15.56 nM (1.59 μg/ml)	Zhang et al. (2017)
7°–9° TFBG-SPR coated with Au film	Cytokeratin 7 full protein CK7FP CK7 peptide	1542	0.2	~7712	500 (assuming the values provided by Voisin et al., 2014)	–	–	CK7FP 1 pM (0.078 ng/ml) CK7 pep 0.4 nM (1.04 ng/ml)	Ribaut et al. (2016)
7° TFBG-SPR coated with Au film	Cytokeratin 17	1543	0.30	~5142	–	–	–	10^{-12} g/mL (0.001 ng/ml)	Ribaut et al. (2017)
10° TFBG-LSPR with Au nanocages and Au nanospheres	Biotin	1538	0.1	~15382	350 (assuming the values provided by Bialiayeu et al., 2011)	1.31–1.34	–	AuNc 8 pM (1.95 pg/ml) AuNs 11 pM (2.69 pg/ml)	Lepinay et al. (2014)
6° TFBG -SPR coated with Au film	Streptavidin Transferrin	1560	0.1	~15600	500 (authors report)	1.32–1.42	5000	Streptavidin: 2 pM (0.11 ng/ml) Transferrin: 10^{-7} g/ml (0.1 μg/ml)	Voisin et al. (2014)

Table 2
Analysed parameters for LPFG-based optical fiber biosensors. Excessively tilted FBGs can be considered as a specific case of LPFGs, as mentioned in section 2.1.2. The sensitivity in DTP-LPFGs has been obtained by tracking the separation of both bands at DTP, which typically increases the sensitivity of each single band by a factor of 2.

Substrate	Biomarker	λ_0 (nm)	FWHM (nm)	Q-factor	Sensitivity (nm/RIU)	RIU range	FOM (RIU^{-1})	Limit of detection	Reference
LPFG	AmpC β- lactamase	1635	12.11	-135	~1500		124	few tens of nM	(Quero et al., 2016b)
LPFG	Bacterial lipopolysaccharide	1612	21	-76.76	6900	–	328.57	0.6 uM	Brzozowska et al. (2015)
LPFG	DNA	1590	15	~106	–	–	–	2 μM (9.22 μg/ml)	Chen et al. (2007)
LPFG	Streptavidin	1429	19	~75.16	–		–	< 0.0125 mg/ml	Wang et al. (2009)
LPFG	Streptavidin	1635	17	~96.18	1000		58.8	0.1 mg/ml	Pilla et al. (2009)
LPFG with policarbonate and graphene oxide	Biotinylated BSA	1575	5	~315	2000	1.334	400	< 0.2 aM (0.01 fg/ml)	Esposito et al. (2018)
LPFG with atactic polystyrene	Tg	1617	3	~539	~1700	1.34	566.67	0.08 ng/ml	(Quero et al., 2016a)
LPFG	*Anti*-IgG	–	–	–	15	1.33	–	0.5, 7.6 mg/l (500, 7600 ng/ml)	Chiavaioli et al. (2014b)
LPFG with titania-silica	*Anti*-IgG	1535	15	~102.33	A −2044.5 B −7075.3	1.333–1.334	472	A 25 μg/l (25 ng/ml) B 13 μg/l (13 ng/ml) C (Serum) 8 μg/l (8 ng/ml)	Chiavaioli et al. (2015)
LPFG with silica-titania	*Anti*-IgG	1575	4.4	~358	7000	1.33–1.34	1590	0.025 mg/l (25 ng/ml)	Biswas et al. (2017)
DTP-LPFG	DNA	1535	1	~1535	154	–	154	10 nM (~46 ng/ml)	Delgado-Pinar et al. (2017)
DTP-LPFG	IgG	1500	15	~100	1309	1.333–1.393	87.27	50 ng/ml	Chiavaioli et al. (2014a)
DTP-LPFG with graphene oxide	*Anti*-IgG	1320	19	~69.47	2538	1.333–1.347	133.58	7 ng/ml	Liu et al. (2017)
DTP-LPFG	DNA	1420	5.79	~245.25	1359	1.30–1.44	137.13	4 nM (~18.4 ng/ml)	Chen Liu (2015)
DTP-LPFG	*E. coli* B (Bacteria)	–	–	–	3000	1.3–1.5	–	10^7 cfu/ml	(Krans, 2015)
~81° TFBG coated with Au nanospheres	Newcastle disease virus (NDV)	1585	6	~264	~180	1.33–1.38	~30	25 pg/mL (0.025 ng/ml)	Luo et al. (2018)
~81° TFBG	Porcine circovirus type 2	1545	1.5	~1030	135	1.33–1.38	90	4.06 ng/ml	Luo et al. (2016)

Table 3
Analysed parameters for interferometry-based optical fiber biosensors. All-fiber interferometers and Fabry-Pérot structures are included.

Substrate	Biomarker	λ_0 (nm)	FWHM (nm)	Q-factor	Sensitivity (nm/RIU)	RIU range	FOM (RIU^{-1})	Limit of detection	Reference
SMF – PCF – SMF	Streptavidin	1552	10	~155.2	320	1.33–1.34	32	10 μg/ml	Hu et al. (2012)
SMF – PCF – SMF	*Anti*-BSA	1545	14	-110.36	722.3	1.308–1.320	51.59	125 pg/ml (0.125 ng/ml)	Betancur-Ochoa et al. (2017)
SMF – exposed core fiber – SMF	Streptavidin	1360	26.7	~50.94	- 3137	1.332–1.335	117.5	–	(Lee et al., 2018)
In-fiber MZI (half SMF core)	BSA	1500	9.8	~153	−10055	1.300–1.330	1026	2.57×10^{-4} mg/ml (257 ng/ml)	Li et al. (2017)
SMF (core mismatch)	IgG	1625	120	~13.54	~14000	1.332–1.339	116.66	47 ng/ml	(B. T. Wang and Wang, 2018a)
Etched SMS	*Anti*-IgG	1380	10	~138	280	1.32–1.41	28	0.2 mg/L (200 ng/ml)	Cardona-Maya et al. (2018)
Chitosan nickel-coated SMS	Histidine tagged proteins	1570	10	-157	69.12	–	6.9	0.8368 ng/ml	Ravikumar et al. (2018)
Nonadiabatic tapered SMF combined with FBG (FBG for temperature control)	Breast cancer biomarker (HER2)	1527	10	~152.7	2333	1.332–1.344	233.3	2 ng/ml	Sun et al. (2017)
Polymer-coated nonadiabatic tapered SMF	DNA	1498	4	374.5	–	–	–	$< 10^{-10}$ M (0.79 ng/ml)	Huang et al. (2000)
Tapered capillary optofluidic sensor	μRNA	1530	10.71	~142.86	1300	–	121.38	212 pM (1.43 ng/ml)	Liang et al. (2017)
FPI	BSA	1565	25.4	~61.61	–		–	0.48 ng	Chen et al. (2012)

Table 4
Analysed parameters for resonance-based optical fiber biosensors. SPR, LSPR and LMRs are included.

Substrate	Biomarker	λ_0 (nm)	FWHM (nm)	Q-factor	Sensitivity (nm/RIU)	RIU range	FOM (RIU^{-1})	Limit of detection	Reference
SPR with Au nano-disks array on optical fiber tip	Prostate cancer biomarker (f-PSA)	700	142.86	-4.9	-226	–	1.58	100 fg/ml	Sanders et al. (2014)
LSPR with Au nanorods	Ochratoxin A	800	137.5	-5.81	601.05	1.333–1.442	4.37	12.0 pM (0.0048 ng/ml)	Lee et al. (2018)
SPR with Au nanopattern on optical fiber tip	*Anti*-BSA	-890	6.6	134.8	595	1.341–1.368	60.7 (authors report)	–	Jia and Yang (2014)
SPR + LSPR with Au on MMF – PCF – MMF	IgG	–	–	–	3915	1.333–1.373	–	37 ng/ml	(B. T. Wang and Wang, 2018b)
SPR with Ag + graphene oxide	IgG	525	–	–	3311	1.333–1.373	24 (authors report)	40 ng/ml	(Q. Wang and Wang, 2018)
LSPRs with Au nanospheres and with nanorods on optical fiber tip	Anti-human IgG	(GNs) 600 (GNr) 875	–	–	(GNs) 914 (GNr) 601	1.33–1.4	–	1.6 nM (240 ng/ml)	Cao et al. (2013)
SPR with electroless plated Au film	IgG	694	108.2 (authors report)	6.41	2054	1.333–1.359	19 (authors report)	0.9 µg/ml	Shi et al. (2015)
LMR with ITO and with SnO_2	*Anti*-IgG	(ITO) 570 (SnO_2) 1490	(ITO) 85 (SnO_2) 50	(ITO)- 6.7 (SnO_2)- 29.8	(ITO) 600 (SnO_2) 14000	–	(ITO) 7.06 (SnO_2) 280	MMF ITO: 3.5 ng/ml (23 pM) MMF SnO_2: 0.9 ng/ml (6 pM) SMF: 0.15 ng/l (1 fM)	Chiavaioli et al. (2018)
LMR with ITO	C reactive protein	1370	12	-180.25	6000	1.335	500	0.0625 ng/ml	Zubiate et al. (2017)

nanoparticles, as indicated in Table 1.

Regarding LPFGs, the other major group presented in section 2 as a suitable candidate for biosensing, one of the first works on a biosensing application based on this structure consisted of a standard LPFG in which the fibre surface was functionalized by using methacrylic acid/methacrylate copolymer (Eudragit® 100) for the implementation of an IgG/*anti*-IgG bioassay. The results showed a sensitivity of 15 nm/RIU and an LOD of 500 ng/ml *anti*-IgG (Chiavaioli et al., 2014b). Later, the same authors presented a ten-fold performance enhancement by using an LPFG operating in the dispersion turning point (DTP). With this structure it was possible to obtain a Q-factor of 100, a sensitivity of 1309 nm/RIU, an FOM of 87.27 RIU^{-1} and an LOD of 50 ng/ml (Chiavaioli et al., 2014a). Additionally, by applying the mode transition phenomenon, the same group designed sol – gel based titania – silica-coated LPFGs, where a significant FOM, sensitivity and LOD improvement was reported: 472 RIU^{-1}, 7075.3 nm/RIU and 8 ng/ml respectively for *anti*-IgG (Chiavaioli et al., 2015) and 1590 RIU^{-1}, 7000 nm/RIU and 25 ng/ml for *anti*-IgG (Biswas et al., 2017). The functionalization of the DTP-LPFG using graphene oxide nanosheets, tested by a different group, resulted in similar sensitivity and LOD results: 2538 nm/RIU and 7 ng/ml of *anti*-IgG (Liu et al., 2017), proving the fine performance of coated DTP-LPFGs. Moreover, an LPFG biosensor coated with a single layer of atactic polystyrene allowed the detection of thyroglobulin, a protein biomarker of differentiated thyroid cancer, with Q 539, 1690 nm/RIU of sensitivity and FOM 566.6 RIU^{-1} (Quero et al., 2016). LPFG-based biosensors have also been used for biotin/streptavidin binding detection (Esposito et al., 2018; Lepinay et al., 2014; Liu et al., 2018; Pilla et al., 2009; Voisin et al., 2014; Wang et al., 2009), while the lowest LOD was obtained with a reflection configuration, resulting in an LOD of 0.01 fg/ml of biotinylated BSA (Esposito et al., 2018), though it must be stated that the size of the molecule plays a role in this low LOD achieved.

Another important application domain of biosensors is the detection of nucleic acids, which are employed as biomarkers with diverse applications, including diagnosis, prognosis and selection of targeted therapies. Currently, publications on the wavelength-based optical fibre biosensors for nucleic acids are scarce, but there are some papers that evidence the interest of the scientific community in the topic. The most sensitive optical structure among the different fibre gratings optical platforms used to detect specific sequences of DNA was DTP-LPFG (1359 nm/RIU), which reported the lowest LOD: 4 nM (~18.4 ng/ml) of DNA (Chen Liu, 2015).

4.2. Optical fibre biosensors based on interferometers

Among interferometers, an etched single-mode multimode single-mode (E-SMS) optical fibre structure has proved to be an effective and suitable optical platform for IgG/*anti*-IgG detection bioassays, with a Q 138, 280 nm/RIU sensitivity, 28 RIU^{-1} FOM and 200 ng/ml *anti*-IgG LOD (Cardona-Maya et al., 2018) (Fig. 12). Here, due to the fact of obtaining a periodic spectrum with several resonant bands available, a dual measurement in both wavelength shift and phase is presented. A better sensitivity was obtained using a single-mode fibre with a longer core-offset fusion splice based on an in-fibre MZI. This platform presented a high sensitivity (13936 nm/RIU) and low LOD (47 ng/ml *anti*-IgG) (Wang and Wang, 2018). Furthermore, an immunosensor based on the Fabry–Pérot interferometer with a layer-by-layer (chitosan/polystyrene sulfonate) membrane was also used to detect the *anti*-IgG. In this case, an LOD of 0.78 ng/ml *anti*-IgG was obtained (Chen et al., 2013).

In addition, in-fibre MZIs have also been used for BSA/*anti*-BSA biosensing. For instance, with a photonic crystal fibre taper an LOD of 0.125 ng/ml of *anti*-BSA was obtained (Betancur-Ochoa et al., 2017), while the sensitivity was 722.3 nm/RIU and the FOM 51.59 RIU^{-1}. In another contribution based on an in-fibre MZI created on the core of an SMF fibre, a higher FOM (1026 RIU^{-1}) and a sensitivity of 10055 nm/

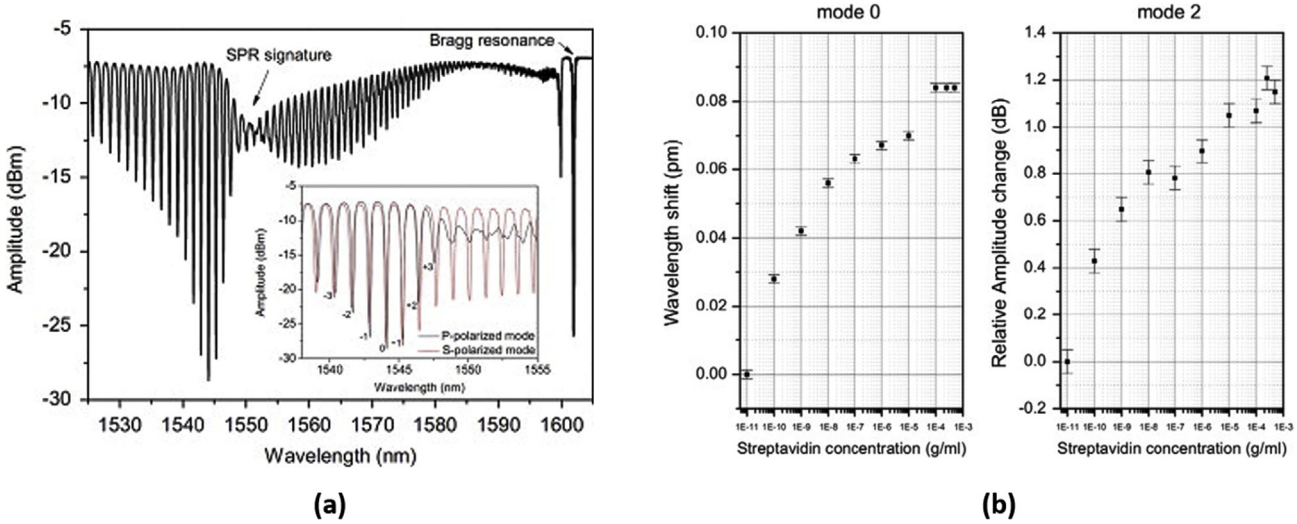

Fig. 11. (a) Transmitted spectrum of a TFBG-SPR immersed in salted water (SRI around 1.38) with its corresponding electrical and magnetic components. (b) Wavelength shift and amplitude sensorgrams for 0 and + 2 modes as a function of streptavidin concentration. Reproduced with permission of Elsevier (Voisin et al., 2014) with Creative Commons Attribution License (CC BY 4.0).

RIU was obtained. However, the LOD increased: 257 ng/ml of BSA (Li et al., 2017). In addition, a PCF-based in-fibre MZI was used for biotin/streptavidin detection, achieving a similar sensitivity of 320 nm/RIU and lower FOM: 32 RIU^{-1} (Hu et al., 2012). The LOD reported with this platform was 10 μg/ml of streptavidin (10000 ng/ml). The differences among these three biosensing platforms as well as in the characteristics of the analyte and its affinity to the bioreceptors are assumed to be the reasons for the varying LOD results. In addition, in the three cases the detected analyte was different: antiBSA, BSA and streptavidin respectively (see Table 3).

Optical fibre biosensors based on interferometers have also been used in the detection of nucleic acids. A taper interferometer achieved $< 10^{-10}$ M (0.79 ng/ml) LOD for a specific sequence of DNA (Huang et al., 2000). In the case of the microRNA, the optical structure employed was a modal interferometer, which achieved a sensitivity of 1300 nm/RIU and allowed the detection of 1.43 ng/ml of microRNA (Liang et al., 2017).

4.3. Optical fibre biosensors based on resonances

Regarding biosensors based on resonances, the generation of SPRs with metallic nanostructures deposited on fibre is one of the most

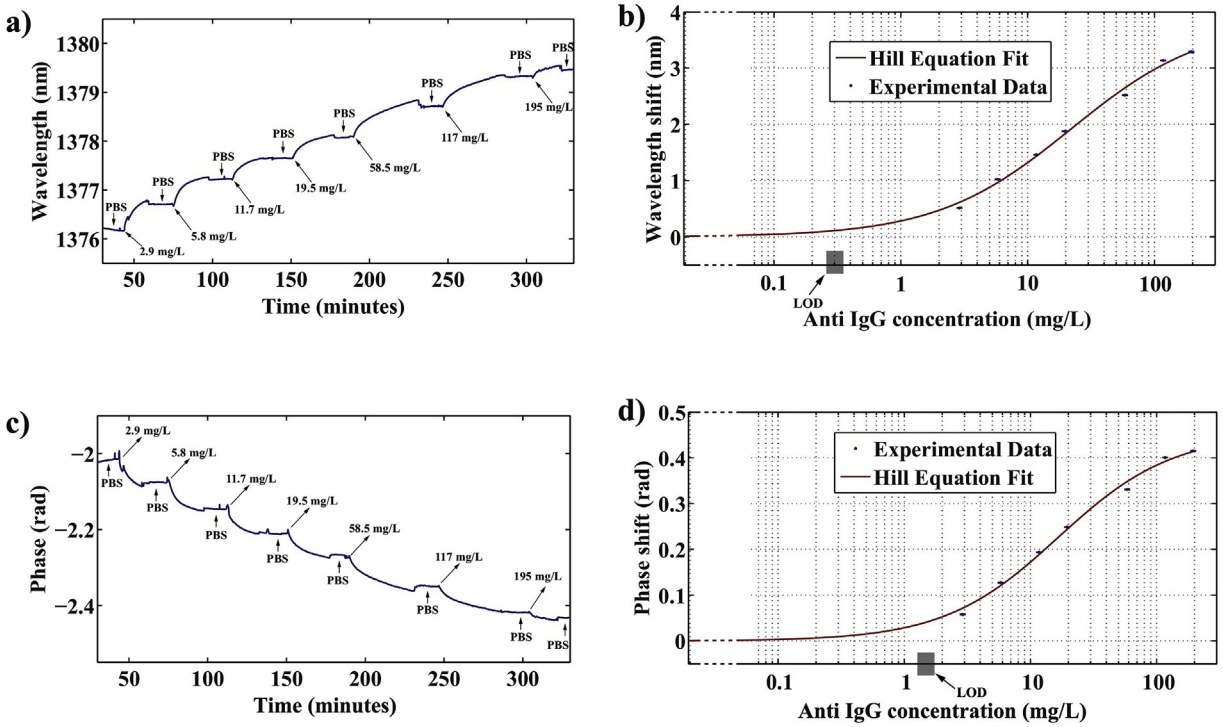

Fig. 12. Results corresponding to bioassay E-SMS 1 with different concentrations of goat *anti*-IgG, ranging from 2.9 mg/l to 195 mg/L a) Wavelength response curve, b) calibration curve in wavelength. The solid line provides the best sigmoidal curve fitting of the experimental data with a 0.9981 correlation coefficient, c) phase response curve, d) calibration curve of the phase shift. The solid line represents the best curve fitting for the sigmoidal Hill equation with a 0.9980 correlation coefficient. Reproduced with permission of Elsevier (Cardona-Maya et al., 2018) with Creative Commons Attribution License (CC BY 4.0).

studied techniques (Lin et al., 2010). In spite of this, in most SPR sensors based on optical fibre, the values of Q and FOM obtained are quite low, because of the broad spectral width of the resonances. That is why it is more common to find SPRs in combination with other techniques (Caucheteur et al., 2017; Lepinay et al., 2014; Ribaut et al., 2017, 2016; Voisin et al., 2014; Zhang et al., 2017) or with some improvements.

In particular, LSPRs have found application in the detection of biological agents with a very low LOD. The implementation of an LSPR optical fibre biosensor has been successfully used for detection of *anti*-BSA (Jia and Yang, 2014), a mycotoxin called ochratoxin A (Lee et al., 2018) and free prostate specific antigen cancer biomarker (Sanders et al., 2014). The parameters obtained with this optical platform were in the same order of magnitude in the different papers. The Q-factor value was around 6 in the case of ochratoxin A and free prostate cancer biomarker (Lee et al., 2018; Sanders et al., 2014). In addition, the sensitivity was ~ 600 nm/RIU in the detection of *anti*-BSA and ochratoxin A (Jia and Yang, 2014; Lee et al., 2018) and ~ 226 nm/RIU in the case of free prostate specific antigen detection (Sanders et al., 2014). These optical fibre biosensors allow the detection of 4.8 pg/ml of ochratoxin A (Lee et al., 2018) and 0.1 pg/ml of free prostate specific antigen (Sanders et al., 2014).

Regarding LMRs, a comparison was done on the performance of uncladded 200-micron-core silica fibres and D-shape SMF fibres coated with indium tin oxide (ITO) or tin dioxide (SnO_2) (Chiavaioli et al., 2018) (Fig. 13a). The nanocoating that shows the best performance is SnO_2, whereas the best optical structure is D-shaped SMF, with a sensitivity of 14000 nm/RIU (Arregui et al., 2016) and an LOD of 0.15 pg/ml (Chiavaioli et al., 2018). This result improves on the best value obtained with uncladded 200-micron-core silica fibres (0.9 ng/ml) by three orders of magnitude (see Fig. 13b and c). In addition, the detection of C-reactive protein, an inflammation process biomarker, by ITO-coated D-shape SMF fibre reported 6000 nm/RIU sensitivity, 500 RIU^{-1} FOM and 0.0625 ng/ml LOD (Zubiate et al., 2017) (see Table 4).

4.4. Comparative study of parameters among biosensing platforms

After presenting the performance of the different optical structures, it is time to compare the different biosensing optical platforms with the aid of the parameters within Tables 1–4 Table 1 refers to TFBGs. Though TFBGs with higher tilt angles present moderate values of FOM (below 100 RIU^{-1}), the rest of the TFBGs present Q values of the order of 10^3 and 10^4, but their inherent sensitivity is very low, which is inadequate for obtaining high FOM values. However, the deposition of either gold thin-films or nanoparticles allows the sensitivity to be increased and FOMs exceeding 10^4 RIU^{-1} can be obtained.

The Q-factor achieved by LPFG-based optical structures ranges from 10^2 to 10^3, one order of magnitude lower than TFBGs. However, the sensitivity is of the order of hundreds to thousands of nm/RIU, which makes it possible to achieve FOMs of up to 1590 RIU^{-1} (Biswas et al., 2017), very close to the values obtained with the best TFBGs. Moreover, this value was just achieved with the mode transition (MT) phenomenon. If both MT and DTP were combined, this value could probably be improved, though it must be pointed out that in the DTP region the spectral width is typically increased (Del Villar et al., 2018).

Interferometers are the most heterogeneous group because of the wide differences among the different optical platforms. Their Q is in the range of hundreds and the sensitivity is quite variable, with a couple of specific cases with 10000 (Li et al., 2017) and 14000 nm/RIU (Wang and Wang, 2018), whereas the FOM is in the range of hundreds of RIU^{-1} with an exceptional case of 1026 RIU^{-1} (Li et al., 2017).

A last technology for developing biosensors includes those structures based on resonances (SPRs, LSPRs or LMRs). They normally present low Q-factors. However, the sensitivity of LMRs is very high, achieving values of 14000 nm/RIU in the water region in the case of nanocoated D-shaped fibres (Arregui et al., 2016). This fine property, combined with the improvement in the Q-factor by controlling the polarization of light, allows FOM values of 280 and 500 RIU^{-1} to be obtained (Chiavaioli et al., 2018; Zubiate et al., 2017).

The best devices in terms of sensitivity can be found in Table 4 (SPRs and LMRs), with several structures that exceed 1000 nm/RIU and

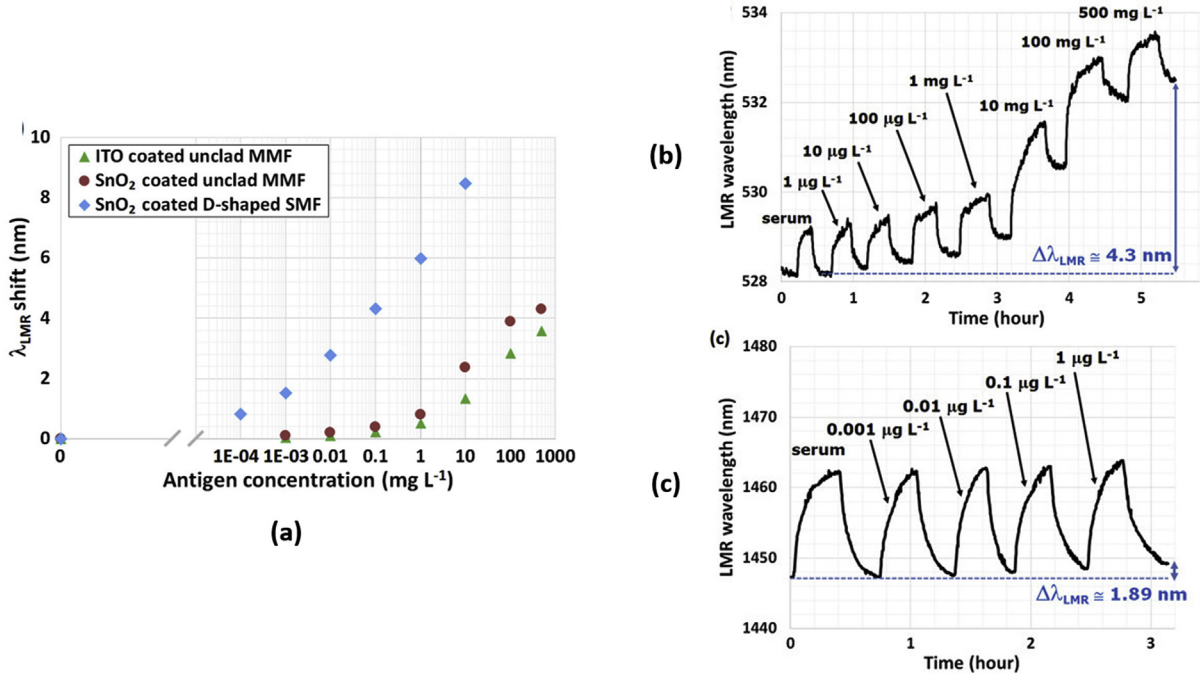

Fig. 13. (a) Comparison among calibration curves obtained with three kinds of LMR sensors: ITO-coated (triangles) and SnO_2-coated (circles) unclad MMF biosensors, and the SnO_2-coated D-shaped SMF biosensor (rhombuses). (b) Sensorgram of the SnO_2-coated unclad MMF biosensor starting from serum to all antigen concentrations (1 µg/l – 500 mg/l). (c) Sensorgram of the SnO_2-coated D-shaped SMF biosensor starting from the serum to all the antigen concentrations (0.001 µg/l – 1 µg/l). Reprinted with permission from (Chiavaioli et al., 2018). Copyright (2018) American Chemical Society.

one reaching 14000 nm/RIU in the water region (Arregui et al., 2016). In Table 3 (interferometers), it is possible to find high sensitivities exceeding 10000 nm/RIU (Wang and Wang, 2018), but there are also other devices with only tens of nm/RIU. In Table 2 (LPFGs), the sensitivities range from 500 to 7000 nm/RIU (the devices are slightly less sensitive than LMRs). Finally, in Table 1 (TFBGs), the sensitivity is reduced to hundreds of nm/RIU in the best cases, when depositing gold thin-films or nanoparticles (Guo, 2017; Voisin et al., 2014).

Although a good parameter, sensitivity becomes a disadvantage if the biosensor film attached to the optical structure is very thick, because a wide spectrum is necessary to monitor the wavelength shift. In this respect, a lower sensitivity is better, as long as the resolution is maintained. Therefore, it is also important to consider either the full width at half maximum (FWHM) or the Q-factor, because both of them are related to the smallest wavelength shift that can be detected. Of these two parameters, the Q-factor, as stated in section 3, minimizes the influence of the operating wavelength. That is why the focus will be centred on this parameter instead of the FWHM. Regarding the Q-factor, according to Tables 1–4 it is clear that the order of best performance observed when analysing sensitivity is inverted. Specifically, TFBGs (the Q ranges from 10^3 to 10^4), LPFGs (the Q ranges from 10^2 to 10^3), interferometers (the Q is typically 10^2) and resonances (the Q ranges from 10^1 to 10^2) is the ranking obtained.

Apparently, TFBGs seem to be the best devices for biosensing in that they present a very high Q-factor and an acceptable sensitivity. However, cost is another important issue. Devices with a high Q-factor require detectors with a very high resolution that can be used for tracking very small wavelength shifts. Considering that question, resonance-based sensors are easier to apply in a system with a detector of low resolution. That is why many authors use the FOM, a parameter that balances the importance of the sensitivity and the FWHM (closely related to the Q-factor). Considering this parameter, the order observed for the Q-factor is not modified when analysing the best device in each group: TFBGs (5000 RIU^{-1}), LPFGs (1590 RIU^{-1}), interferometers (1026 RIU^{-1}) and LMR-SPRs (500 RIU^{-1}). However, it must be pointed out that the differences have been diminished compared with the Q-factor.

After understanding that the FOM balances the sensitivity and the Q factor, the final step is to identify the relationship between the FOM and the LOD by comparing biosensors developed in different laboratories. This is a difficult task because there are many additional parameters that play a role in the final results. Despite all this, *anti*-IgG allowed some specific cases to be seen where the FOM is an optical parameter related with the LOD. When detecting *anti*-IgG, an SMS etching interferometer-based biosensor achieved a 28 RIU^{-1} FOM and a 200 ng/ml LOD (Cardona-Maya et al., 2018), whereas with titania–silica-coated LPFG an improvement in the FOM up to 472 RIU^{-1} (Chiavaioli et al., 2015) and to 1590 RIU^{-1} (Biswas et al., 2017) resulted in lower LOD of 8 ng/ml (Chiavaioli et al., 2015) and 25 ng/ml (Biswas et al., 2017) respectively. However, it must be pointed out that if the two LPFG structures are compared, the FOM of the first one is lower than the second one and the opposite is true if they are compared in terms of LOD.

Perhaps the best proof that the FOM is a good assessment parameter for the performance of a biosensor can be found in (Chiavaioli et al., 2018), where two comparisons were made. The first one was the utilization of the same structure, a cladding removed multimode fibre, coated with ITO and with SnO_2. With ITO, a material of lower refractive index than SnO_2 and, consequently, lower sensitivity, a 3.5 ng/ml LOD was obtained, whereas with SnO_2 a 0.9 ng/ml LOD was achieved. Moreover, the application of a D-shaped structure coated with SnO_2, with a higher sensitivity than the cladding removed multimode fibre, allowed a 0.15 pg/ml LOD to be attained. In other words, using a D-shaped fiber and a SnO_2 coating permitted to improve the LOD by more than three orders of magnitude compared to the cladding removed multimode fibre coated with ITO. This was due to the improvement obtained in terms of sensitivity and the FOM. The sensitivity and FOM were improved from 600 nm/RIU and 7 RIU^{-1} with the cladding removed multimode fibre coated with ITO, to 14000 nm/RIU and 280 RIU^{-1} with the D-shaped structure coated with SnO_2.

The relationship between the LOD and the FOM indicates that the FOM is a good parameter for testing optical structures used as biosensors. However, probably in the future, with more publications and data (optical fibre biosensors is a technology that has exploded during the last years), it will be possible to use a more accurate expression parameter than the ratio between sensitivity and FWHM, which is the one used by some authors nowadays (Gupta et al., 2015; Ozcariz et al., 2017). For example, it could be possible that the squared sensitivity divided by the FWHM offers a better prediction of the performance of the optical structures when used for biosensing. In this respect, there is a lot of work to do. This review has analysed this question in terms of FOM in order to compare the performance of the most important optical fibre structures, which will serve to give designers an idea of what type of structure they should use.

5. Conclusions

In summary, this work has presented a review of the most representative scientific contributions on wavelength-based optical fibre biosensors. In first place, according to the literature, the most prominent technologies addressing this topic are: grating-based optical fibres (tilted-FBGs and LPFGs), interferometers (in-fibre Mach–Zehnder interferometers mainly) and resonances (SPRs, LSPRs and LMRs). All of them are based on the generation of resonant bands, either because their own optical structure generates them or because a nanostructured material has been deposited onto the optical substrate to generate or enhance the performance of such resonant band.

Second, a classification of these main optical structures has been made according to several parameters related to the optical structure: full width at half maximum/minimum (FWHM), Q-factor, sensitivity, figure of merit (FOM) and limit of detection (LOD). In terms of sensitivity the ranking from better to worse performance is: resonances, interferometers, LPFGs and TFBGs. However, this ranking is inverted regarding the Q-factor: TFBGs, LPFGs, interferometers and resonances. Also, the ranking is maintained when the FOM is studied, though the differences are diminished because the FOM depends both on the FWHM (closely related to the Q-factor) and on the sensitivity.

The relationship between a high FOM and a low LOD is difficult to establish if different works are compared, since the experimental conditions are different. However, in those works where the conditions are the same it has been proved that improving the FOM allows attaining a better LOD. Consequently, FOM becomes a valid parameter for assessing the performance of an optical structure as a biosensor. It is possible that in the future, with more research, it will be possible to find a more exact parameter to achieve this purpose. At the moment, FOM is a good indicator that can be used to compare the performance of the optical platforms, as has been done in this work.

Declaration of interests

The authors declare that they have no known competing financial interests or personal relationships that could have appeared to influence the work reported in this paper.

CRediT authorship contribution statement

A.B. Socorro-Leránoz: Formal analysis, Investigation, Writing - original draft, Writing - review & editing, Resources, Supervision, Validation. **D. Santano:** Formal analysis, Investigation, Writing - original draft, Writing - review & editing. **I. Del Villar:** Funding acquisition, Resources, Supervision, Validation, Writing - review & editing. **I.R. Matias:** Funding acquisition, Resources, Supervision, Validation,

Writing - review & editing.

Acknowledgements

This work was supported by the Regional Government of Navarra, Spain (projects with references 72/2015 and PC021-022) and by the Agencia Estatal de Investigación (Spanish National Research Agency) through the project with reference TEC2016-78047-R.

References

Abdallah, A., 2018. Experimental study on an interferometric strain sensor based on hollow-core photonic bandgap fibre for intrusion detection. Optic Commun. 428, 35–40. https://doi.org/10.1016/j.optcom.2018.07.035.

Albert, J., Shao, L.-Y., Caucheteur, C., 2013. Tilted fibre Bragg grating sensors. Laser Photonics Rev. https://doi.org/10.1002/lpor.201100039.

Alvarez, M., Lechuga, L.M., 2010. Microcantilever-based platforms as biosensing tools. Analyst 135, 827. https://doi.org/10.1039/b908503n.

Andreev, A., Pantchev, B., Danesh, P., Zafirova, B., Karakoleva, E., Vlaikova, E., Alipieva, E., 2005. A refractometric sensor using index-sensitive mode resonance between single-mode fibre and thin film amorphous silicon waveguide. Sensor. Actuator. B Chem. 106, 484–488. https://doi.org/10.1016/j.snb.2004.09.002.

Anemogiannis, E., Glytsis, E.N., Gaylord, T.K., 2003. Transmission characteristics of long-period fibre gratings having arbitrary azimuthal/radial refractive index variations. J. Light. Technol. 21, 218–227. https://doi.org/10.1109/JLT.2003.808637.

Arnold, M.A., 1985. Enzyme-based fibre optic sensor. Anal. Chem. 57, 565–566. https://doi.org/10.1021/ac50001a055.

Arregui, F.J., Del Villar, I., Zamarreño, C.R., Zamarreño, Z., Zubiate, P., Matias, I.R., 2016. Giant sensitivity of optical fibre sensors by means of lossy mode resonance. Sensor. Actuator. B 232, 660–665. https://doi.org/10.1016/j.snb.2016.04.015.

Batchman, T.E., McWright, G.M., 1982. Mode coupling between dielectric and. IEEE J. Quantum Electron QE-18.

Betancur-Ochoa, J.E., Minkovich, V.P., Montagut-Ferizzola, Y.J., 2017. Special photonic crystal modal interferometer for highly sensitive biosensing. J. Light. Technol. 35, 4747–4751. https://doi.org/10.1109/JLT.2017.2761738.

Bialiayeu, A., Caucheteur, C., Ahamad, N., Ianoul, A., Albert, J., 2011. Self-optimized metal coatings for fibre plasmonics by electroless deposition. Optic Express 19, 18742. https://doi.org/10.1364/OE.19.018742.

Biswas, P., Chiavaioli, F., Jana, S., Basumallick, N., Trono, C., Giannetti, A., Tombelli, S., Mallick, A., Baldini, F., Bandyopadhyay, S., 2017. Design, fabrication and characterisation of silica-titania thin film coated over coupled long period fibre gratings: towards bio-sensing applications. Sensor. Actuator. B Chem. https://doi.org/10.1016/j.snb.2017.06.139.

Boudoux, C., 2017. Fundamentals of Biomedical Optics: from Light Interactions with Cells to Complex Imaging Systems.

Brzozowska, Ewa, Śmietana, Mateusz, Koba, Marcin, Górska, Sabina, Pawlik, Krzysztof, Gamian, Andrzej, Bock, Wojtek J., 2015. Recognition of bacterial lipopolysaccharide using bacteriophage-adhesin-coated long-period gratings. Biosensors and Bioelectronics 67, 93–99. https://doi.org/10.1016/j.bios.2014.07.027.

Budinski, V., Donlagic, D., 2017. Fibre-optic sensors for measurements of torsion, twist and rotation: a review. Sensors 17, 1–29. https://doi.org/10.3390/s17030443.

Cao, Jie, Tu, Minh Hieu, Sun, Tong, Grattan, Kenneth T.V., 2013. Wavelength-based localized surface plasmon resonance optical fiber biosensor. Sensors and Actuators B 181, 611–619. https://doi.org/10.1016/j.snb.2013.02.052.

Cardona-Maya, Y., Del Villar, I., Socorro, A.B., Corres, J.M., Matias, I.R., Botero-Cadavid, J.F., 2017. Wavelength and phase detection based SMS fibre sensors optimized with etching and nanodeposition. J. Light. Technol. https://doi.org/10.1109/JLT.2017.2719923.

Cardona-Maya, Y., Socorro, A.B., Del Villar, I., Cruz, J.L., Corres, J.M., Botero-Cadavid, J.F., 2018. Label-free wavelength and phase detection based SMS fibre immunosensors optimized with cladding etching. Sensor. Actuator. B Chem. https://doi.org/10.1016/j.snb.2018.03.002.

Carneiro, P., Loureiro, J., Delerue-Matos, C., Morais, S., do Carmo Pereira, M., 2017. Alzheimer's disease: development of a sensitive label-free electrochemical immunosensor for detection of amyloid beta peptide. Sensor. Actuator. B Chem. 239, 157–165. https://doi.org/10.1016/j.snb.2016.07.181.

Carotenuto, B., Ricciardi, A., Micco, A., Amorizzo, E., Mercieri, M., Cutolo, A., Cusano, A., 2018. Smart optical catheters for epidurals. Sensors 18, 1–9. https://doi.org/10.3390/s18072101.

Caucheteur, C., Mégret, P., 2005. Demodulation technique for weakly tilted fibre Bragg grating refractometer. IEEE Photonics Technol. Lett. https://doi.org/10.1109/LPT.2005.859411.

Caucheteur, C., Ribaut, C., Malachovska, V., Wattiez, R., 2017. Immunosensing with near-infrared plasmonic optical fibre gratings. https://doi.org/10.1007/978-1-4939-6848-0_4 47–71.

Chan, C.-F., Chen, C., Jafari, A., Laronche, A., Thomson, D.J., Albert, J., 2007. Optical Fibre Refractometer Using Narrowband Cladding-Mode Resonance Shifts.

Chen, J.-H., Zhao, J.-R., Huang, X.-G., Huang, Z.-J., 2010. Extrinsic fibre-optic Fabry-Perot interferometer sensor for refractive index measurement of optical glass. Appl. Opt. 49, 5592–5596. https://doi.org/10.1364/AO.49.005592.

Chen, Li Han, Ang, Xiu Min, Chan, Chi Chiu, Shaillender, Mutukumaraswamy, Neu, Björn, Wong, Wei Chang, Zu, Peng, Leong, Kam Chew, July/August 2012. Layer-By-Layer (Chitosan/Polystyrene Sulfonate) Membrane-Based Fabry–Perot Interferometric Fiber Optic Biosensor. IEEE Journal of Selected Topics in Quantum Electronics 18 (4), 1457–1464. https://doi.org/10.1109/JSTQE.2012.2185221.

Chen, L.H., Chan, C.C., Menon, R., Balamurali, P., Wong, W.C., Ang, X.M., Hu, P.B., Shaillender, M., Neu, B., Zu, P., Tou, Z.Q., Poh, C.L., Leong, K.C., 2013. Fabry-Perot fibre-optic immunosensor based on suspended layer-by-layer (chitosan/polystyrene sulfonate) membrane. Sensor. Actuator. B Chem. https://doi.org/10.1016/j.snb.2013.06.093.

Chen Liu, X.C., 2015. EDC-mediated oligonucleotide immobilization on a long period grating optical biosensor. J. Biosens. Bioelectron. 06. https://doi.org/10.4172/2155-6210.1000173.

Chen, X., Zhou, K., Zhang, L., Bennion, I., 2007. Dual-peak long-period fibre gratings with enhanced refractive index sensitivity by finely tailored mode dispersion that uses the light cladding etching technique. Appl. Opt. 46, 451–455. https://doi.org/10.1364/AO.46.000451.

Chen, X., Zhou, K., Zhang, L., Bennion, I., 2005. Optical chemsensor based on etched tilted bragg grating structures in multimode fibre. IEEE Photonics Technol. Lett. https://doi.org/10.1109/LPT.2004.842786.

Cheymol, G., Brichard, B., Villard, J.F., 2011. Fibre optics for metrology in nuclear research reactors—applications to dimensional measurements. IEEE Trans. Nucl. Sci. 58, 1895–1902. https://doi.org/10.1109/TNS.2011.2160356.

Chiavaioli, F., Biswas, P., Trono, C., Bandyopadhyay, S., Giannetti, A., Tombelli, S., Basumallick, N., Dasgupta, K., Baldini, F., 2014a. Towards sensitive label-free immunosensing by means of turn-around point long period fibre gratings. Biosens. Bioelectron. 60, 305–310. https://doi.org/10.1016/j.bios.2014.04.042.

Chiavaioli, F., Biswas, P., Trono, C., Jana, S., Bandyopadhyay, S., Basumallick, N., Giannetti, A., Tombelli, S., Bera, S., Mallick, A., Baldini, F., 2015. Sol-gel-based titania-silica thin film overlay for long period fibre grating-based biosensors. Anal. Chem. https://doi.org/10.1021/acs.analchem.5b01841.

Chiavaioli, F., Gouveia, C.A.J., Jorge, P.A.S., Baldini, F., 2017. Towards a uniform metrological assessment of grating-based optical fibre sensors: from refractometers to biosensors. Biosensors. https://doi.org/10.3390/bios7020023.

Chiavaioli, F., Trono, C., Giannetti, A., Brenci, M., Baldini, F., 2014b. Characterisation of a label-free biosensor based on long period grating. J. Biophot. 7, 312–322. https://doi.org/10.1002/jbio.201200135.

Chiavaioli, F., Zubiate, P., Del Villar, I., Zamarreǹo, C.R., Giannetti, A., Tombelli, S., Trono, C., Arregui, F.J., Matias, I.R., Baldini, F., 2018. Femtomolar detection by nanocoated fibre label-free biosensors. ACS Sens. 3, 936–943. https://doi.org/10.1021/acssensors.7b00918.

Corres, J.M., Villar, I. Del, Arregui, F.J., Matias, I.R., 2015. Analysis of lossy mode resonances on thin-film coated cladding removed plastic fibre. Opt. Lett. https://doi.org/10.1364/OL.40.004867.

Cusano, a., Iadicicco, a., Pilla, P., Contessa, L., Campopiano, S., Cutolo, a., Giordano, M., 2006. Mode transition in high refractive index coated long period gratings. Optic Express 14, 19–34. https://doi.org/10.1371/journal.pone.0125427.

Dash, J.N., Jha, R., Villatoro, J., Dass, S., 2015. Nano-displacement sensor based on photonic crystal fibre modal interferometer. Opt. Lett. https://doi.org/10.1364/OL.40.000467.

Del Villar, I., 2015. Ultrahigh-sensitivity sensors based on thin-film coated long period gratings with reduced diameter, in transition mode and near the dispersion turning point. Optic Express 23, 8389. https://doi.org/10.1364/OE.23.008389.

Del Villar, I., Achaerandio, M., Matías, I.R., Arregui, F.J., 2005. Deposition of overlays by electrostatic self-assembly in long-period fibre gratings. Opt. Lett. 30, 720. https://doi.org/10.1364/OL.30.000720.

Del Villar, I., Arregui, F.J., Zamarreño, C.R., Corres, J.M., Bariain, C., Goicoechea, J., Elosua, C., Hernaez, M., Rivero, P.J., Socorro, A.B., Urrutia, A., Sanchez, P., Zubiate, P., Lopez, D., De Acha, N., Ascorbe, J., Matias, I.R., 2017a. Optical sensors based on lossy-mode resonances. Sensor. Actuator. B Chem. https://doi.org/10.1016/j.snb.2016.08.126.

Del Villar, I., Fuentes, O., Chiavaioli, F., Corres, J.M., Matias, I.R., 2018. Optimized strain long-period fibre grating (LPFG) sensors operating at the dispersion turning point. J. Light. Technol. https://doi.org/10.1109/JLT.2018.2790434.

Del Villar, I., Hernaez, M., Zamarreño, C.R., Sánchez, P., Fernández-Valdivielso, C., Arregui, F.J., Matias, I.R., 2012. Design rules for lossy mode resonance based sensors. Appl. Opt. https://doi.org/10.1364/AO.51.004298.

Del Villar, I., Zamarreño, C.R., Hernaez, M., Arregui, F.J., Matias, I.R., 2010. Lossy mode resonance generation with indium-tin-oxide-coated optical fibres for sensing applications. J. Light. Technol. https://doi.org/10.1109/JLT.2009.2036580.

Del Villar, I., Zubiate, P., Zamarreño, C.R., Arregui, F.J., Matías, I.R., 2017b. Optimization in nanocoated D-shaped optical fibre sensors. Optic Express 25, 10743–10756. https://doi.org/10.1364/OE.25.010743.

Delgado-Pinar, Martina, Shi, Qing, Poveda-Wong, Luis, Delgado-Pinar, Estefanía, Xu, Baojian, Zhao, Jianlog, Luis Cruz, Jose, Andrés, Miguel V., 2017. Oligonucleotide-Hybridization Fiber-Optic Biosensor Using a Narrow Bandwidth Long Period Grating. IEEE Sensors Journal 17 (17), 5503–5509. https://doi.org/10.1109/JSEN.2017.2723759. 1 Sept.1.

Domingues, M.F., Rodriguez, C.A., Martins, J., Tavares, C., Marques, C., Alberto, N., André, P., Antunes, P., 2018. Cost-effective optical fibre pressure sensor based on intrinsic Fabry-Perot interferometric micro-cavities. Opt. Fibre Technol. https://doi.org/10.1016/j.yofte.2018.02.016.

Elosua, C., De Acha, N., Hernaez, M., Matias, I.R., Arregui, F.J., 2015. Layer-by-Layer assembly of a water-insoluble platinum complex for optical fibre oxygen sensors. Sensor. Actuator. B 207, 683–689. https://doi.org/10.1016/j.snb.2014.10.042.

Erdogan, T., 2000. Cladding-mode resonances in short- and long-period fibre grating filters: errata. J. Opt. Soc. Am. A. https://doi.org/10.1364/JOSAA.17.002113.

Erdogan, T., 1997. Fibre grating spectra. J. Lightwave Technol.

Esposito, F., Sansone, L., Taddei, C., Campopiano, S., Giordano, M., Iadicicco, A., 2018. Ultrasensitive biosensor based on long period grating coated with polycarbonate-graphene oxide multilayer. Sensor. Actuator. B Chem. 274, 517–526. https://doi.org/10.1016/j.snb.2018.08.002.

Gharsallah, Z., Najjar, M., Suthar, B., Janyani, V., 2018. High sensitivity and ultra-compact optical biosensor for detection of UREA concentration. Opt. Quant. Electron. https://doi.org/10.1007/s11082-018-1520-2.

Gouveia, C.A.J., Baptista, J.M., Jorge, P.A., 2013. Refractometric optical fibre platforms for label free sensing. In: Arof, S.W.H., H (Eds.), Current Developments in Optical Fibre Technology. Intech. https://doi.org/10.5772/711.

Guo, T., 2017. Fibre Grat. Assis. Surf. Plasmon Reson. 35, 3323–3333.

Guo, T., Liu, F., Liang, X., Qiu, X., Huang, Y., Xie, C., Xu, P., Mao, W., Guan, B.O., Albert, J., 2016. Highly sensitive detection of urinary protein variations using tilted fibre grating sensors with plasmonic nanocoatings. Biosens. Bioelectron. https://doi.org/10.1016/j.bios.2015.11.047.

Guo, T., Tam, H.-Y., Krug, P.A., Albert, J., 2009. Reflective Tilted Fibre Bragg Grating Refractometer Based on Strong Cladding to Core Recoupling.

Gupta, B.D., Srivastava, S.K., Verma, R., 2015. Fibre Optic Sensors Based on Plasmonics. World Scientific Publishing Co. Pte. Ltd.

Hawk, R.M., Armani, A.M., 2015. Label free detection of 5'hydroxymethylcytosine within CpG islands using optical sensors. Biosens. Bioelectron. https://doi.org/10.1016/j.bios.2014.10.041.

Hernández-Romano, I., Cruz-Garcia, M.A., Moreno-Hernández, C., Monzón-Hernández, D., López-Figueroa, E.O., Paredes-Gallardo, O.E., Torres-Cisneros, M., Villatoro, J., 2016. Optical fibre temperature sensor based on a microcavity with polymer overlay. Optic Express. https://doi.org/10.1364/OE.24.005654.

Holzinger, M., Le Goff, A., Cosnier, S., 2014. Nanomaterials for biosensing applications: a review. Front. Chem. 2, 63. https://doi.org/10.3389/fchem.2014.00063.

Homola, J., Yee, S.S., Gauglitz, G., 1999. Surface plasmon resonance sensors: review. Sensor. Actuator. B Chem. 54, 3–15. https://doi.org/10.1016/S0925-4005(98)00321-9.

Hou, W., Liu, G., Han, M., 2015. A novel, high-resolution, high-speed fibre-optic temperature sensor for oceanographic applications. In: 2015 IEEE/OES Eleventh Current, Waves and Turbulence Measurement (CWTM). IEEE, pp. 1–4. https://doi.org/10.1109/CWTM.2015.7098149.

Hu, D.J.J., Lim, J.L., Park, M.K., Kao, L.T.H., Wang, Y., Wei, H., Tong, W., 2012. Photonic crystal fibre-based interferometric biosensor for streptavidin and biotin detection. IEEE J. Sel. Top. Quantum Electron. 18, 1293–1297. https://doi.org/10.1109/JSTQE.2011.2169492.

Huang, Y., Tian, Z., Sun, L.-P., Sun, D., Li, J., Ran, Y., Guan, B.-O., Steemers, F.J., Ferguson, J.A., Walt, D.R., Wu, N., Zou, X., Wang, X., Papadakis, G., Tsortos, A., Bender, F., Ferapontova, E.E., Gizeli, E., Solis, A., Coq, D.L., Juncker, C., Riley, M.R., Collier, J., Boesewetter, D.E., Boussard-Pledel, C., 2000. High-sensitivity DNA biosensor based on optical fibre taper interferometer coated with conjugated polymer tentacle. 2. Y. Tian, W". Sensors 18, 1854–1861. https://doi.org/10.1364/OE.23.026962.

Islam, M., Ali, M.M., Lai, M.H., Lim, K.S., Ahmad, H., 2014. Chronology of fabry-perot interferometer fibre-optic sensors and their applications: a review. Sensors. https://doi.org/10.3390/s140407451.

James, S.W., Tatam, R.P., 2003. Optical fibre long-period grating sensors: characteristics and application. Meas. Sci. Technol.

Jatschka, J., Dathe, A., Csáki, A., Fritzsche, W., Stranik, O., 2016. Propagating and localized surface plasmon resonance sensing - a critical comparison based on measurements and theory. Sens. Bio Sens. Res. https://doi.org/10.1016/j.sbsr.2016.01.003.

Jia, P., Yang, J., 2014. A plasmonic optical fibre patterned by template transfer as a high-performance flexible nanoprobe for real-time biosensing. Nanoscale 6, 8836–8843. https://doi.org/10.1039/c4nr01411a.

Jiang, B., Lu, X., Gan, X., Qi, M., Wang, Y., Han, L., Mao, D., Zhang, W., Ren, Z., Zhao, J., 2015. Graphene-coated tilted fibre-Bragg grating for enhanced sensing in low-refractive-index region. Opt. Lett. 40, 3994. https://doi.org/10.1364/ol.40.003994.

Jiang, N., Ahmed, R., Rifat, A.A., Guo, J., Yin, Y., Montelongo, Y., Butt, H., Yetisen, A.K., 2018. Functionalized flexible soft polymer optical fibres for laser photomedicine. Adv. Opt. Mater. 6, 1–10. https://doi.org/10.1002/adom.201701118.

Jung, Y., Kim, S., Lee, D., Oh, K., 2006. Compact three segmented multimode fibre modal interferometer for high sensitivity refractive-index measurement. In: Measurement Science and Technology, . https://doi.org/10.1088/0957-0233/17/5/S32.

Krans, B., 2015. Endoscopy, healthline [WWW document]. Endosc. Heal. http://www.healthline.com/health/endoscopy.

Laffont, G., Ferdinand, P., 2001. Tilted short-period fibre-Bragg-grating-induced coupling to cladding modes for accurate refractometry. Meas. Sci. Technol. 12, 765–770. https://doi.org/10.1088/0957-0233/12/7/302.

Lee, B., Park, J.H., Byun, J.Y., Kim, J.H., Kim, M.G., 2018. An optical fibre-based LSPR aptasensor for simple and rapid in-situ detection of ochratoxin A. Biosens. Bioelectron. 102, 504–509. https://doi.org/10.1016/j.bios.2017.11.062.

Lepinay, S., Staff, A., Ianoul, A., Albert, J., 2014. Improved detection limits of protein optical fibre biosensors coated with gold nanoparticles. Biosens. Bioelectron. 52, 337–344. https://doi.org/10.1016/j.bios.2013.08.058.

Leung, A., Shankar, P.M., Mutharasan, R., 2012. Evanescent field tapered fibre optic biosensors (TFOBS): fabrication, antibody immobilization and detection. In: Schlesinger, J.C. (Ed.), Optical Fibres Research Advances.

Li, Z., Liao, C., Chen, D., Song, J., Jin, W., Peng, G.-D., Zhu, F., Wang, Y., He, J., Wang, Y., 2017. Label-free detection of bovine serum albumin based on an in-fibre Mach-Zehnder interferometric biosensor. Optic Express 25, 17105. https://doi.org/10.1364/OE.25.017105.

Liang, L., Jin, L., Ran, Y., Sun, L.P., Guan, B.O., 2017. Interferometric detection of microRNAs using a capillary optofluidic sensor. Sensor. Actuator. B Chem. 242, 999–1006. https://doi.org/10.1016/j.snb.2016.09.153.

Liang, W., Huang, Y., Xu, Y., Lee, R.K., Yariv, A., 2005. Highly sensitive fibre Bragg grating refractive index sensors. Appl. Phys. Lett. 86, 1–3. https://doi.org/10.1063/1.1904716.

Liedberg, B., Nylander, C., Lundström, I., 1995. Biosensing with Surface Plasmon Resonance-How it All Started, Bioanalytical History Report.

Lin, Y., Zou, Y., Mo, Y., Guo, J., Lindquist, R.G., 2010. E-beam patterned gold nanodot arrays on optical fibre tips for localized surface plasmon resonance biochemical sensing. Sensors 10, 9397–9406. https://doi.org/10.3390/s101009397.

Lismont, M., Vandewalle, N., Joris, B., Dreesen, L., 2014. Fibre based optofluidic biosensors. Appl. Phys. Lett. 105. https://doi.org/10.1063/1.4896767.

Liu, C., Cai, Q., Xu, B., Zhu, W., Zhang, L., Zhao, J., Chen, X., 2017. Graphene oxide functionalized long period grating for ultrasensitive label-free immunosensing. Biosens. Bioelectron. https://doi.org/10.1016/j.bios.2017.03.004.

Liu, C., Xu, B.J., Zhou, L., Sun, Z., Mao, H.J., Zhao, J.L., Zhang, L., Chen, X., 2018. Graphene oxide functionalized long period fibre grating for highly sensitive hemoglobin detection. Sensor. Actuator. B Chem. 261, 91–96. https://doi.org/10.1016/j.snb.2018.01.117.

Liu, Z., Wei, Y., Zhang, Y., Wang, Y., Zhao, E., Zhang, Y., Yang, J., Liu, C., Yuan, L., 2016. A multi-channel fibre SPR sensor based on TDM technology. Sensor. Actuator. B Chem. 226, 326–331. https://doi.org/10.1016/j.snb.2015.11.102.

Lopez-Torres, D., Lopez-Aldaba, A., Elosua, C., Auguste, J.L., Jamier, R., Roy, P., Lopez-Amo, M., Arregui, F.J., 2018. Comparison between different structures of suspended-core microstructured optical fibres for volatiles sensing. Sensors 18. https://doi.org/10.3390/s18082523.

Luna-Moreno, D., Monzón-Hernández, D., Villatoro, J., Badenes, G., 2007. Optical fibre hydrogen sensor based on core diameter mismatch and annealed Pd-Au thin films. Sensor. Actuator. B Chem. https://doi.org/10.1016/j.snb.2007.01.036.

Luo, B., Wu, S., Zou, W., Zhang, Z., Zhao, M., Shi, S., Liu, Y., Xi, X., Zeng, Z., Liang, W., Yan, Z., Zhang, L., 2016. Label-free immunoassay for porcine circovirus type 2 based on excessively tilted fibre grating modified with staphylococcal protein A. Biosens. Bioelectron. 86, 1054–1060. https://doi.org/10.1016/j.bios.2016.07.100.

Luo, B., Xu, Y., Wu, S., Zhao, M., Jiang, P., Shi, S., Zhang, Z., Wang, Y., Wang, L., Liu, Y., 2018. A novel immunosensor based on excessively tilted fibre grating coated with gold nanospheres improves the detection limit of Newcastle disease virus. Biosens. Bioelectron. 100, 169–175. https://doi.org/10.1016/j.bios.2017.08.064.

Luo, D., Ma, J., Ibrahim, Z., Ismail, Z., 2017. Etched FBG coated with polyimide for simultaneous detection the salinity and temperature. Optic Commun. https://doi.org/10.1016/j.optcom.2016.12.068.

Marciniak, M., Grzegorzewski, J., Szustakowski, M., 1993. Analysis of lossy mode cut-off conditions in planar waveguides with semiconductor guiding layer. IEEE Proc. J. Optoelectron. 140, 247. https://doi.org/10.1049/ip-j.1993.0040.

Martyn-Hemphill, C., Chandrasekera, S., Muir, G., 2017. Surgical treatment: green light laser. In: The Big Prostate, . https://doi.org/10.1007/978-3-319-64704-3_8.

Mishra, S.K., Usha, S.P., Gupta, B.D., 2016. A lossy mode resonance-based fibre optic hydrogen gas sensor for room temperature using coatings of ITO thin film and nanoparticles. Meas. Sci. Technol. https://doi.org/10.1088/0957-0233/27/4/045103.

Monton, M.R.N., Forsberg, E.M., Brennan, J.D., 2012. Tailoring sol-gel-derived silica materials for optical biosensing. Chem. Mater. 24, 796–811. https://doi.org/10.1021/cm202798e.

Nabok, A., Al-Rubaye, A.G., Al-Jawdah, A.M., Tsargorodska, A., Marty, J.L., Catanante, G., Szekacs, A., Takacs, E., 2019. [INVITED] Novel optical biosensing technologies for detection of mycotoxins. Optic Laser. Technol. https://doi.org/10.1016/j.optlastec.2018.07.076.

Ozcariz, A., Zamarreño, C.R., Zubiate, P., Arregui, F.J., 2017. Is there a frontier in sensitivity with Lossy mode resonance (LMR) based refractometers? Sci. Rep. https://doi.org/10.1038/s41598-017-11145-9.

P&S Market Research, 2015. Global Biosensors Market Size, Share, Development, Growth and Demand Forecast to 2022 – Industry Insights by Technology (Electrochemical, Optical, Thermal and Piezoelectric). Application (Medical Testing, Industrial Process, Environment, Agricultural T.

Pérez-Juste, J., Pastoriza-Santos, I., Liz-Marzán, L.M., Mulvaney, P., 2005. Gold nanorods: synthesis, characterization and applications. Coord. Chem. Rev. 249, 1870–1901. https://doi.org/10.1016/j.ccr.2005.01.030.

Pilla, P., Manzillo, P.F., Malachovska, V., Buosciolo, A., Campopiano, S., Cutolo, A., Ambrosio, L., Giordano, M., Cusano, A., 2009. Long period grating working in transition mode as promising technological platform for label-free biosensing. Optic Express 17, 20039–20050. https://doi.org/10.1364/OE.17.020039.

Pilla, P., Trono, C., Baldini, F., Chiavaioli, F., Giordano, M., Cusano, A., 2012. Giant sensitivity of long period gratings in transition mode near the dispersion turning point: an integrated design approach. Opt. Lett. 37, 4152. https://doi.org/10.1364/OL.37.004152.

Poeggel, S., Tosi, D., Duraibabu, D., Leen, G., McGrath, D., Lewis, E., 2015. Optical fibre pressure sensors in medical applications. Sensors. https://doi.org/10.3390/s150717115.

Pongruengkiat, W., Pechprasarn, S., 2017. Whispering-gallery mode resonators for detecting cancer. Sensors. https://doi.org/10.3390/s17092095.

Principe, M., Consales, M., Micco, A., Crescitelli, A., Castaldi, G., Esposito, E., La Ferrara, V., Cutolo, A., Galdi, V., Cusano, A., 2017. Optical fibre meta-tips. Light Sci. Appl. https://doi.org/10.1038/lsa.2016.226.

Quero, G., Consales, M., Severino, R., Vaiano, P., Boniello, A., Sandomenico, A., Ruvo, M., Borriello, A., Diodato, L., Zuppolini, S., Giordano, M., Nettore, I.C., Mazzarella, C., Colao, A., Macchia, P.E., Santorelli, F., Cutolo, A., Cusano, A., 2016. Long period fibre grating nano-optrode for cancer biomarker detection. Biosens. Bioelectron. 80, 590–600. https://doi.org/10.1016/j.bios.2016.02.021.

Radan, S., Homola, J., 2006. Letter to the Editor Ultrahigh resolution long range surface plasmon-based sensor. https://doi.org/10.1016/j.snb.2006.08.020.
Ravikumar, Raghunandhan, Chen, Li Han, Jayaraman, Premkumar, Loo Poh, Chueh, Chan, Chi Chiu, 2018. Chitosan-nickel film based interferometric optical fiber sensor for label-free detection of histidine tagged proteins. Biosensors and Bioelectronics 99, 578–585. https://doi.org/10.1016/j.bios.2017.08.012.
Ribaut, C., Loyez, M., Larrieu, J.C., Chevineau, S., Lambert, P., Remmelink, M., Wattiez, R., Caucheteur, C., 2017. Cancer biomarker sensing using packaged plasmonic optical fibre gratings: towards in vivo diagnosis. Biosens. Bioelectron. 92, 449–456. https://doi.org/10.1016/j.bios.2016.10.081.
Ribaut, C., Voisin, V., Malachovská, V., Dubois, V., Mégret, P., Wattiez, R., Caucheteur, C., 2016. Small biomolecule immunosensing with plasmonic optical fibre grating sensor. Biosens. Bioelectron. 77, 315–322. https://doi.org/10.1016/j.bios.2015.09.019.
Rivero, P.J., Goicoechea, J., Hernaez, M., Socorro, A.B., Matias, I.R., Arregui, F.J., 2016. Optical fibre resonance-based pH sensors using gold nanoparticles into polymeric layer-by-layer coatings. Microsyst. Technol. 22, 1821–1829. https://doi.org/10.1007/s00542-016-2857-8.
Rivero, P.J., Urrutia, A., Goicoechea, J., Matias, I.R., Arregui, F.J., 2013. A Lossy Mode Resonance optical sensor using silver nanoparticles-loaded films for monitoring human breathing. Sensor. Actuator. B Chem. 187, 40–44. https://doi.org/10.1016/j.snb.2012.09.022.
Rodriguez-Cobo, L., Cobo, A., Lopez-Higuera, J.-M., 2014. Optical strain gauge with high spatial resolution. J. Strain Anal. Eng. Des. https://doi.org/10.1177/0309324714529282.
Rosenthal, A., Kellnberger, S., Bozhko, D., Chekkoury, A., Omar, M., Razansky, D., Ntziachristos, V., 2014. Sensitive interferometric detection of ultrasound for minimally invasive clinical imaging applications. Laser Photonics Rev. 8, 450–457. https://doi.org/10.1002/lpor.201300204.
Rycenga, M., Cobley, C.M., Zeng, J., Li, W., Moran, C.H., Zhang, Q., Qin, D., Xia, Y., 2011. Controlling the synthesis and assembly of silver nanostructures for plasmonic applications. Chem. Rev. 111, 3669–3712. https://doi.org/10.1021/cr100275d.
Sanders, M., Lin, Y., Wei, J., Bono, T., Lindquist, R.G., 2014. An enhanced LSPR fiber-optic nanoprobe for ultrasensitive detection of protein biomarkers. Biosens. Bioelectron. 61, 95–101. https://doi.org/10.1016/j.bios.2014.05.009.
Shafiee, H., Lidstone, E.A., Jahangir, M., Inci, F., Hanhauser, E., Henrich, T.J., Kuritzkes, D.R., Cunningham, B.T., Demirci, U., 2014. Nanostructured optical photonic crystal biosensor for HIV viral load measurement. Sci. Rep. https://doi.org/10.1038/srep04116.
Shi, Se, Wang, Libing, Su, Rongxin, Liu, Boshi, Huang, Renliang, Qi, Wei, He, Zhimin, 2015. A polydopamine-modified optical fiber SPR biosensor using electroless-plated gold films for immunoassays. Biosensors and Bioelectronics 74, 454–460. https://doi.org/10.1016/j.bios.2015.06.080.
Shu, X., Zhu, X., Jiang, S., Shi, W., Huang, D., 1999. High sensitivity of dual resonant peaks of long-period fibre grating to surrounding refractive index changes. Electron. Lett. 35, 1580. https://doi.org/10.1049/el:19991040.
Silva, S., Pachon, E.G.P., Franco, M.A.R., Hayashi, J.G., Malcata, F.X., Frazão, O., Jorge, P., Cordeiro, C.M.B., 2012. Ultrahigh-sensitivity temperature fibre sensor based on multimode interference. Appl. Opt. https://doi.org/10.1364/AO.51.003236.
Śmietana, M., Koba, M., Mikulic, P., Bock, W.J., 2016. Towards refractive index sensitivity of long-period gratings at level of tens of μm per refractive index unit: fibre cladding etching and nano-coating deposition. Optic Express 24, 11897. https://doi.org/10.1364/OE.24.011897.
Śmietana, M., Sobaszek, M., Michalak, B., Niedziałkowski, P., Białobrzeska, W., Koba, M., Sezemsky, P., Stranak, V., Karczewski, J., Ossowski, T., Bogdanowicz, R., 2018. Optical monitoring of electrochemical processes with ITO-based lossy-mode resonance optical fibre sensor applied as an electrode. J. Light. Technol. 36, 954–960. https://doi.org/10.1109/JLT.2018.2797083.
Socorro, A.B., Corres, J.M., Del Villar, I., Arregui, F.J., Matias, I.R., 2012. Fibre-optic biosensor based on lossy mode resonances. Sensor. Actuator. B Chem. 174, 263–269. https://doi.org/10.1016/j.snb.2012.07.039.
Socorro, A.B., Del Villar, I., Corres, J.M., Arregui, F.J., Matias, I.R., 2014a. Sensitivity enhancement in a multimode interference-based SMS fibre structure coated with a thin-film: theoretical and experimental study. Sensor. Actuator. B Chem. https://doi.org/10.1016/j.snb.2013.08.090.
Socorro, A.B., Del Villar, I., Corres, J.M., Arregui, F.J., Matias, I.R., 2014b. Spectral width reduction in lossy mode resonance-based sensors by means of tapered optical fibre structures. Sensor. Actuator. B Chem. https://doi.org/10.1016/j.snb.2014.04.017.
Špačkova, B., Wrobel, P., Bockova, M., Homola, J., 2016. Optical biosensors based on plasmonic nanostructures: a review. Proc. IEEE. https://doi.org/10.1109/JPROC.2016.2624340.
Sroka, R., Weick, K., Sadeghi-Azandaryani, M., Steckmeier, B., Schmedt, C.-G., 2010. Endovenous laser therapy–application studies and latest investigations. J. Biophot. 3, 269–276. https://doi.org/10.1002/jbio.200900097.
Sun, D., Ran, Y., Wang, G., 2017. Label-free detection of cancer biomarkers using an in-line taper fibre-optic interferometer and a fibre bragg grating. https://doi.org/10.3390/s17112559.
Tang, Y., Zeng, X., Liang, J., 2010. Surface plasmon resonance: an introduction to a surface spectroscopy technique NIH public access. J. Chem. Educ. 87, 742–746. https://doi.org/10.1021/ed100186y.
Tavousi, A., Rakhshani, M.R., Mansouri-Birjandi, M.A., 2018. High sensitivity label-free refractometer based biosensor applicable to glycated hemoglobin detection in human blood using all-circular photonic crystal ring resonators. Optic Commun. https://doi.org/10.1016/j.optcom.2018.08.019.
Usha, S.P., Mishra, S.K., Gupta, B.D., 2015a. Zinc oxide thin film/nanorods based lossy mode resonance hydrogen sulphide gas sensor. Mater. Res. Express. https://doi.org/10.1088/2053-1591/2/9/095003.
Usha, S.P., Mishra, S.K., Gupta, B.D., 2015b. Fibre optic hydrogen sulfide gas sensors utilizing ZnO thin film/ZnO nanoparticles: a comparison of surface plasmon resonance and lossy mode resonance. Sensor. Actuator. B Chem. 218, 196–204. https://doi.org/10.1016/j.snb.2015.04.108.
Usha, S.P., Shrivastav, A.M., Gupta, B.D., 2018. Semiconductor metal oxide/polymer based fibre optic lossy mode resonance sensors: a contemporary study. Opt. Fibre Technol. https://doi.org/10.1016/j.yofte.2018.07.003.
Vaiano, P., Carotenuto, B., Pisco, M., Ricciardi, A., Quero, G., Consales, M., Crescitelli, A., Esposito, E., Cusano, A., 2016. Lab on Fibre Technology for biological sensing applications. Laser Photonics Rev. https://doi.org/10.1002/lpor.201600111.
Villatoro, J., Monzón-Hernández, D., 2006. Low-cost optical fibre refractive-index sensor based on core diameter mismatch. J. Light. Technol. https://doi.org/10.1109/JLT.2005.863246.
Voisin, V., Pilate, J., Damman, P., Mégret, P., Caucheteur, C., 2014. Highly sensitive detection of molecular interactions with plasmonic optical fibre grating sensors. Biosens. Bioelectron. 51, 249–254. https://doi.org/10.1016/j.bios.2013.07.030.
Wallner, J., Lhota, G., Jeschek, D., Mader, A., Vorauer-Uhl, K., 2013. Application of Bio-Layer Interferometry for the analysis of protein/liposome interactions. J. Pharm. Biomed. Anal. https://doi.org/10.1016/j.jpba.2012.10.008.
Wang, A., Member, S., Xiao, H., Wang, J., Wang, Z., Zhao, W., May, R.G., 2001. Self-calibrated interferometric – intensity-based. Opt. Fibre Sens. 19, 1495–1501.
Wang, B.T., Wang, Q., 2018. An interferometric optical fibre biosensor with high sensitivity for IgG/anti-IgG immunosensing. Optic Commun. https://doi.org/10.1016/j.optcom.2018.05.058.
Wang, Q., Zhao, W.M., 2018. A comprehensive review of lossy mode resonance-based fibre optic sensors. Optic Laser. Eng. https://doi.org/10.1016/j.optlaseng.2017.07.009.
Wang, X.D., Wolfbeis, O.S., 2016. Fibre-optic chemical sensors and biosensors (2013-2015). Anal. Chem. 88, 203–227. https://doi.org/10.1021/acs.analchem.5b04298.
Wang, Y., Huang, Q., Zhu, W., Yang, M., 2018. Simultaneous measurement of temperature and relative humidity based on FBG and FP interferometer. IEEE Photonics Technol. Lett. https://doi.org/10.1109/LPT.2018.2818744.
Wang, Z., Heflin, J.R., Van Cott, K., Stolen, R.H., Ramachandran, S., Ghalmi, S., 2009. Biosensors employing ionic self-assembled multilayers adsorbed on long-period fibre gratings. Sensor. Actuator. B Chem. https://doi.org/10.1016/j.snb.2009.02.073.
Weltin, A., Kieninger, J., Urban, G.A., 2016. Microfabricated, amperometric, enzyme-based biosensors for in vivo applications. Anal. Bioanal. Chem. 408, 4503–4521. https://doi.org/10.1007/s00216-016-9420-4.
Wu, Q., Semenova, Y., Wang, P., Farrell, G., 2011. High sensitivity SMS fibre structure based refractometer–analysis and experiment. Optic Express 19, 7937–7944. https://doi.org/10.1364/OE.19.007937.
Xiong, R., Meng, H., Yao, Q., Huang, B., Liu, Y., Xue, H., Tan, C., Huang, X., 2014. Simultaneous measurement of refractive index and temperature based on modal interference. IEEE Sens. J. https://doi.org/10.1109/JSEN.2014.2310463.
Yadav, T.K., Narayanaswamy, R., Abu Bakar, M.H., Kamil, Y.M., Mahdi, M.A., 2014. Single mode tapered fibre-optic interferometer based refractive index sensor and its application to protein sensing. Optic Express. https://doi.org/10.1364/OE.22.022802.
Yang, F., Sambles, J.R., 1997. Determination of the optical permittivity and thickness of absorbing films using long range modes. J. Mod. Opt. 44, 1155–1163. https://doi.org/10.1080/09500349708230726.
Yang, P., Pang, J., Hu, F., Peng, J., Jiang, D., Chu, Z., Jin, W., 2018. An ultrasensitive biosensing flexible chip using a novel silver@Prussian blue core-shell nanocube composite. Sensor. Actuator. B Chem. 276, 31–41. https://doi.org/10.1016/j.snb.2018.08.070.
Yuan, Z., Hu, C.-C., Chang, H.-T., Lu, C., 2016. Gold nanoparticles as sensitive optical probes. Analyst. https://doi.org/10.1039/C5AN02651B.
Zamarreño, C.R., Hernáez, M., Del Villar, I., Matías, I.R., Arregui, F.J., 2011. Optical fibre pH sensor based on lossy-mode resonances by means of thin polymeric coatings. Sensor. Actuator. B Chem. https://doi.org/10.1016/j.snb.2010.12.037.
Zamarreño, C.R., Socorro, A.B., Sanchez, P., Matias, I.R., Arregui, F.J., 2015. In: Taylor (Ed.), Fibre-optic Biosensors. CRC Press.
Zamarreño, C.R., Zamarreño, Z., Hernaez, M., Del Villar, I., Matias, I.R., Arregui, F.J., 2010. Tunable humidity sensor based on ITO-coated optical fibre. Sensor. Actuator. B 146, 414–417. https://doi.org/10.1016/j.snb.2010.02.029.
Zhang, Y., 2011. Long-range Surface Polaritons in Thin Layer of Absorbing Materials. Technical University of Eindhoven.
Zhang, Y., Wang, F., Qian, S., Liu, Z., Wang, Q., Gu, Y., Wu, Z., Jing, Z., Sun, C., Peng, W., 2017. A novel fibre optic surface plasmon resonance biosensors with special boronic acid derivative to detect glycoprotein. Sensors 17. https://doi.org/10.3390/s17102259.
Zhao, Y., Zhao, H., Lv, R. qing, Zhao, J., 2019. Review of optical fibre Mach–Zehnder interferometers with micro-cavity fabricated by femtosecond laser and sensing applications. Optic Laser. Eng. 117, 7–20. https://doi.org/10.1016/j.optlaseng.2018.12.013.
Zhou, K., Zhang, L., Chen, X., Bennion, I., 2006. Optic sensors of high refractive-index responsivity and low thermal cross sensitivity that use fibre Bragg gratings of > 80° tilted structures. Opt. Lett. 31 (1193). https://doi.org/10.1364/OL.31.001193.
Zhou, W., Li, K., Wei, Y., Hao, P., Chi, M., Liu, Y., Wu, Y., 2018. Ultrasensitive label-free optical microfibre coupler biosensor for detection of cardiac troponin I based on interference turning point effect. Biosens. Bioelectron. 106, 99–104. https://doi.org/10.1016/j.bios.2018.01.061.
Zhou, W., Zhou, Y., Albert, J., 2017. A true fibre optic refractometer. Laser Photonics Rev. 11, 1–10. https://doi.org/10.1002/lpor.201600157.
Zubiate, P., Zamarreno, C.R., Del Villar, I., Matias, I.R., Arregui, F.J., 2015. Experimental

study and sensing applications of polarization-dependent lossy mode resonances generated by D-shape coated optical fibres. J. Light. Technol. https://doi.org/10.1109/JLT.2015.2392791.
Zubiate, P., Zamarreño, C.R., Sánchez, P., Matias, I.R., Arregui, F.J., 2017. High sensitive and selective C-reactive protein detection by means of lossy mode resonance based optical fibre devices. Biosens. Bioelectron. 93, 176–181. https://doi.org/10.1016/j.bios.2016.09.020.

Abián B. Socorro-Leránoz is an Electrical and Electronic Engineer (2010), M.Sc. in Biomedical Engineering (2012) and Ph.D. in Engineering (2015) from the Public University of Navarre (PUN-UPNA), Pamplona, Navarre, Spain. He was at the Armani Research Lab (University of Southern California, Los Angeles, CA, USA) as a visiting Ph.D. student in 2014. Currently, he is working as Assistant Professor at PUN/UPNA, where he has published more than 55 scientific contributions both in JCR journals and conferences and he has been involved in more than 15 competitive research projects with both public and private funding. Most of them have been related to the development of optical fibre sensors and their application to biomedicine.

His research interests are the development of optical fibre sensors, including biosensors and, in general, the development of biomedical applications based on optical fibres.

Desiree Santano Rivero is a Biologist (2013) and received her M.Sc. in Microbiology and Health from the University of the Basque Country (UPV/EHU), Spain. She has co-authored conference papers related to Microbiology and Biomedical Engineering. Currently, she is working as researcher at PUN/UPNA.

Her research interests focus on the biomedical engineering field, including the development of optical fibre biosensors.

Ignacio Del Villar received his M.S. degree in Electrical and Electronic Engineering and his Ph.D. degree, specialising in Optical Fibre Sensors, in 2002 and 2006, respectively from the Public University of Navarra (UPNA). During 2004 he was a visiting scientist at the Institute d'Optique (Orsay, France) and in 2005 he was a visiting scientist at the Applied Physics Department of the University of Valencia (Burjassot, Spain). He is presently a Reader at the UPNA since 2008, an Associate Editor of the Optics & Laser Technology Journal since 2012 and an Associate Editor of the Journal of Sensors since 2014.

His research interests include optical fibre sensors and the analysis of waveguides and nanostructured materials, where he has co-authored more than 100 book chapters, journals and conference papers.

Ignacio R. Matias received the M.S. degree in Electrical and Electronic Engineering and his Ph.D. degree in Optical Fibre Sensors from the Polytechnic University of Madrid (UPM), Spain, in 1992 and 1996, respectively. He became a Lecturer at the Public University of Navarra (Pamplona, Spain) in 1996, where he is presently a Permanent Professor. He has co-authored more than 300 book chapters, journals and conference papers related to optical fibre sensors and passive optical devices and systems. He was co-Founding Editor of the IEEE Sensors Journal. He is an IEEE Senior member.